

# ***Method of Moments Applied to Antennas***

***Tapan K. Sarkar***

Department of Electrical and Computer Engineering, Syracuse University, N.Y. 13244-1240, USA.

***Antonije R. Djordjevic***

***Branko M. Kolundzija***

School of Electrical Engineering, University of Belgrade, 11120 Belgrade, Yugoslavia.

November 2000



## *Table of Contents*

Method of Moments Applied to Antennas.....	i
1. Introduction.....	1
2. Maxwell's equations.....	3
2.1. Basic equations, constitutive relations, and boundary conditions.....	3
2.2. Phasor representation and equations in complex domain.....	4
2.3. Lorentz potentials and Green's function.....	6
3. Method of moments.....	8
3.1. Linear operator equations.....	8
3.2. Basic steps of the method of moments.....	8
3.3. Formulation of integral equations.....	11
3.4. Example.....	12
4. Antenna analysis.....	14
4.1. Introduction.....	14
4.2. Wire antennas.....	15
4.2.1. Definition of wire antennas.....	15
4.2.2. Integral equations and their solution.....	15
4.2.3. Two-potential equation.....	16
4.2.4. Evaluation of antenna characteristics.....	18
4.2.5. Examples.....	20
4.3. Metallic (surface) antennas.....	22
4.3.1. Definition of metallic antennas.....	22
4.3.2. Integral equations and their solution.....	23
4.3.3. Examples.....	26
4.4. Metallo-dielectric antennas.....	27
4.4.1. Definition of metallo-dielectric antennas.....	27
4.4.2. Volume integral equation and its solution.....	28
4.4.3. Surface integral equations and their solution.....	30
4.4.4. Finite-element method.....	31
4.4.5. Example.....	32
5. Conclusion.....	32
6. Acknowledgment.....	33
7. References.....	34



# 1. Introduction

The art of the electrical engineering design partly relies on the ability to properly model the physical structure under consideration. A good model enables an efficient and accurate analysis, so that the designer can reach his/her goal with a few iterations on the model and, usually, a few steps of experimental verification.

Most electrical and electronic engineers use circuit-theory models to analyze various passive and active circuits. Such models are simple and straightforward to implement, they do not require bulky theoretical background, and they are easy to visualize. However, they may fail to predict circuit behavior even at power frequencies, let alone analyze radiation phenomena. Let us not forget that the circuit-theory models need a link to the physical structure they represent to provide meaningful results. For example, we need to know how to evaluate the resistance of a wire to represent it by a resistor.

Electromagnetic field models are predominantly used by antenna and microwave engineers. The analysis starts from the physical structure (i.e., the geometry and electrical properties of materials involved), and it gives a full insight into the properties of devices and circuits (including propagation, radiation, parasitic effects, etc.). Most electromagnetic field problems do not have an analytical solution and a numerical approach is required. However, writing a computer code for the solution of a class of problems is a hard task. Even to properly use codes for the electromagnetic field analysis, a lot of background and experience is required. This software is usually very sophisticated, it covers only a narrow region of applications, and it may sometimes require a long central processor unit (CPU) time to produce results.

An efficient and accurate computer simulation of various electromagnetic field problems, including antennas, is made possible by modern fast computers and well-developed numerical techniques. This simulation enables an antenna designer to visualize the targeted antenna on the desktop, providing in many cases more information than can ever be measured in the laboratory or *in situ*, at a lower cost and higher efficiency. A good personal computer and appropriate software may cost significantly less than antenna measurement instrumentation required to equip an antenna laboratory. The turn-around time required to obtain antenna properties after changing antenna shape or dimensions is usually measured by minutes or hours for a computer simulation, but it may require days to build a new antenna prototype and perform measurements. The designer can tune the antenna by modifying certain parameters of the simulation model (e.g., antenna dimensions, material properties, etc.), and thus faithfully reflect results he/she would be getting in the laboratory by trimming the antenna structure. The accuracy of available numerical models is often such that only a small degree of adjustment is required, if any, on the laboratory prototype or on the final product. However, proper interpretation of computed results is necessary, bearing in mind inherent limitations of the technique applied. Hence, a proper selection and evaluation of the computer code is a prerequisite for obtaining reliable results. In many cases, users strive for user-friendly programs, which have ample graphics input and output capabilities, and even include movies. However, in code evaluation, it is more important to be sure that the implemented models can be applied to the actual problem to be solved, and that results can be obtained with a sufficient speed and accuracy.

There exists a variety of numerical methods for the analysis of electromagnetic fields. They are based on the solution of Maxwell's equations or certain equations derived from them. Maxwell's equations are fundamental equations for electromagnetic fields [1] and they can be in integral or differential form. Maxwell's equations are revealed in Section 2 of this chapter.

The numerical methods for field analysis can be classified in a variety of ways. Most numerical techniques deal with linear systems, as are most antenna structures. Such systems can always be described in terms of linear operator equations. An operator is a mapping of a function space to a function space [2]. Hence, the unknown in an operator equation is a function. Some techniques deal with nonlinear systems, but they are not within our scope here.

Another classification is based on the quantity that is solved for in the numerical technique (further referred as the unknown quantity), as follows.

One group of methods directly solves for the electric or magnetic field vectors, or for quantities tightly related with them (e.g., the Lorentz potentials). The starting equations are Maxwell's equations in differential form or their derivatives (e.g., the wave equation). The unknowns are, hence, spread throughout the volume occupied by the fields. For linear media, as we assume in this chapter, the resulting equations are linear partial differential equations in terms of the unknowns. To this group belong the finite-element method (FEM) and the finite-difference (FD) method. The latter method includes, for example, the technique for solving the Laplace equation in electrostatics and the finite-difference time-domain technique described in another chapter of this book. Both the FEM and FD are relatively straightforward to program, and they can handle highly inhomogeneous and even nonlinear media. However, they usually require a lot of spatial and temporal samples to provide a satisfactory accuracy, and, consequently, they demand large computer resources.

The second group of methods solves for the field sources (currents and charges). These sources can be either physical sources, or mathematical (equivalent) sources introduced through various electromagnetic field theorems [3,4]. In the numerical analysis, the electromagnetic fields, or the related potentials, are expressed in terms of these sources, usually through the Lorentz potentials. The expressions are integral forms, where the sources appear under some integrals, multiplied by appropriate functions, which are referred to as kernels. For example, for fields in a vacuum, the kernel for the Lorentz potentials is the free-space Green's function. On the other hand, certain equations are imposed based on the boundary conditions or constitutive relations. The boundary conditions relate tangential and normal components of the field vectors at a surface of discontinuity. For example, on the surface of a perfectly conducting body, the tangential component of the electric field vanishes. The constitutive equations reflect material properties: dielectric polarization, current conduction, and magnetization. Finally in the derivation, the quantities involved in the boundary conditions and constitutive relations are expressed in terms of the field sources. As the result, an integral equation (or a set of integral equations) is obtained for the unknown sources. For linear media, as assumed here, these integral equations are linear. In some cases, the unknowns are distributed through a volume, like the d.c. currents and associated charges in a conducting medium. In many other cases, the sources are distributed only over surfaces, thus depending on two local coordinates (e.g., scattering from a thin metallic plate in a vacuum), or along lines, thus depending on one local coordinate (e.g., a wire antenna). The resulting equations are integral equations in terms of the unknowns, though, in some cases, derivatives of the unknowns may appear somewhere in the equation. The techniques of this group are most often based on the method of moments (MoM), which is the main topic of this chapter. As a rule, techniques of this group require a lot of analytical preparation and implementation of sophisticated numerical procedures. They are usually inefficient when applied to highly inhomogeneous media, and they are not applicable to nonlinear media.

Combinations of these two groups of methods are also possible. They are referred to as hybrid methods, and they can combine the respective advantages of each group. Thereby, the differential equation formulation is applied to highly inhomogeneous (and possibly anisotropic and nonlinear) regions, and the integral equation formulation for the remaining space.

At this place, a remark should be made on the dimensionality of the electromagnetic fields and unknowns. An electromagnetic field is always a three-dimensional spatial phenomenon, meaning that it exists within a finite or infinite region (volume). In most cases, the field vectors are functions of three spatial coordinates (e.g., the Cartesian  $x$ ,  $y$ , and  $z$  coordinates), and such problems are referred to as three-dimensional (3D) electromagnetic field problems. In some problems, the fields are functions of only two coordinates. For example, the electrostatic field of an infinitely long two-wire line depends only on the transverse coordinates. The related problems are referred to as two-dimensional (2D) problems. Even simpler cases are when the fields depend only on one spatial coordinate. For example, the electric and magnetic fields of a uniform plane wave depend only on the longitudinal coordinate. In such cases we speak about one-dimensional (1D) problems.

The dimensionality of an electromagnetic field problem should not be confused with the mathematical dimensionality of the unknowns. They may or may not coincide. For example, when the unknowns are fields in a 3D electromagnetic problem, the unknowns are also functions of three spatial coordinates, and we have a 3D mathematical problem. However, if we solve for the field sources, the situation may be different. For example, if we analyze scattering from a rectangular metallic plate in a vacuum, the unknowns are currents induced on the plate, which depend on two local coordinates associated with the plate. Hence, the unknowns constitute a 2D mathematical problem. If we consider scattering from a thin wire in a vacuum, the unknown is the current distribution along the wire, and we have an 1D mathematical problem.

For the analysis in the time domain, the temporal variable increases the mathematical dimensionality of the problem by one. In this chapter, however, we deal exclusively with the frequency-domain analysis.

Efficiency of a numerical solution significantly depends on the mathematical dimensionality of the unknowns. In most cases, faster and more accurate solutions are obtained when the dimensionality is smaller.

The stress in this chapter is on the application of integral equations to antenna problems, and their solution using the MoM. In Section 3 the basic philosophy of the MoM is presented, without going into details, and omitting rigorous proofs. An interested reader should refer to several excellent books [2,5-15] for an in-depth coverage of the MoM. In Section 4 specifics of the MoM application to antennas are presented. This section is further divided into three parts, according to the increased complexity of structures analyzed. Section 4.2 deals with wire antennas, Section 4.3 deals with arbitrarily shaped metallic structures, whereas Section 4.4 is devoted to the most general case – combined metallic and dielectric structures. In Sections 3 and 4 illustrative examples are given showing various possibilities of the MoM.

## 2. Maxwell's equations

### 2.1. Basic equations, constitutive relations, and boundary conditions

Maxwell's equations are general equations that govern macroscopic electromagnetic fields. In the time domain, in differential form, the four basic Maxwell's equations read [1]:

$$\text{curl } \mathbf{E} = -\frac{\partial \mathbf{B}}{\partial t}, \quad \text{curl } \mathbf{H} = \mathbf{J} + \frac{\partial \mathbf{D}}{\partial t}, \quad \text{div } \mathbf{D} = \rho, \quad \text{div } \mathbf{B} = 0, \quad (1)$$

where  $\mathbf{E}$  is the electric field intensity,  $\mathbf{H}$  the magnetic field intensity,  $\mathbf{D}$  the electric flux density (also referred to as the electric displacement or the electric induction),  $\mathbf{B}$  the magnetic flux density (also referred to as the magnetic induction),  $\mathbf{J}$  the electric current density, and  $\rho$  the volume charge density. All quantities in equation (1) depend on the position-vector ( $\mathbf{r}$ ) and time ( $t$ ). To obtain a complete system, the four basic equations should be complemented by constitutive relations, which read in the general form:

$$\mathbf{D} = \mathbf{D}(\mathbf{E}), \quad \mathbf{J} = \mathbf{J}(\mathbf{E}), \quad \mathbf{B} = \mathbf{B}(\mathbf{H}). \quad (2)$$

In particular, for linear media,

$$\mathbf{D} = \varepsilon \mathbf{E}, \quad \mathbf{J} = \sigma \mathbf{E} + \mathbf{J}_i, \quad \mathbf{B} = \mu \mathbf{H}, \quad (3)$$

where  $\varepsilon$  is the permittivity,  $\sigma$  the conductivity, and  $\mu$  the permeability of the medium, whereas  $\mathbf{J}_i$  is the density of impressed electric currents, which model the excitation. The excitation in equation (3) corresponds to a current generator in the circuit theory. The impressed currents create an electromagnetic field, just like ordinary electric currents. The excitation can alternatively be modeled by the impressed electric field,  $\mathbf{E}_i$ , using the relation  $\mathbf{J} = \sigma(\mathbf{E} + \mathbf{E}_i)$ , which corresponds to a voltage generator in the circuit theory.

In practical electromagnetic field problems, the geometry and constitutive parameters of the structure are usually given along with the excitation, and the objective is to evaluate other quantities of interest.

From the second and third equation in (1), the continuity equation can be derived,

$$\text{div } \mathbf{J} = -\frac{\partial \rho}{\partial t}. \quad (4)$$

In the circuit theory, the continuity equation corresponds to Kirchhoff's current law.

Equations (1) and (4) are valid provided the vectors  $\mathbf{E}$ ,  $\mathbf{H}$ ,  $\mathbf{D}$ ,  $\mathbf{B}$ , and  $\mathbf{J}$  are differentiable functions of the position-vector. These vectors may not be differentiable at an interface surface between two media (which differ in parameters  $\varepsilon$ ,  $\sigma$ , or  $\mu$ ), shown in Figure 1. At such an interface, instead of Maxwell's equations in differential form, fields satisfy boundary conditions. These conditions are relations between tangential and normal components of the field vectors. They are expressed in vector form as

$$\mathbf{n} \times \mathbf{E}_1 - \mathbf{n} \times \mathbf{E}_2 = 0, \quad \mathbf{n} \times \mathbf{H}_1 - \mathbf{n} \times \mathbf{H}_2 = \mathbf{J}_s, \quad \mathbf{n} \cdot \mathbf{D}_1 - \mathbf{n} \cdot \mathbf{D}_2 = \rho_s, \quad \mathbf{n} \cdot \mathbf{B}_1 - \mathbf{n} \cdot \mathbf{B}_2 = 0, \quad (5)$$

where  $\mathbf{n}$  is the unit normal directed from medium 1 towards medium 2,  $\mathbf{J}_s$  is the density of surface currents, and  $\rho_s$  the density of surface charges on the interface.

Note that integral form of Maxwell's equations is more general than differential form, and equations (1) and (5) are directly derivable from integral form. However, differential form is more convenient for our present needs.

A perfect electric conductor (PEC) is a fictitious conductor whose conductivity ( $\sigma$ ) is infinitely large. In such a medium, there can not exist time-dependent electromagnetic fields. Hence, if medium 2 is a PEC, equations (5) reduce to

$$\mathbf{n} \times \mathbf{E}_1 = 0, \quad \mathbf{n} \times \mathbf{H}_1 = \mathbf{J}_s, \quad \mathbf{n} \cdot \mathbf{D}_1 = \rho_s, \quad \mathbf{n} \cdot \mathbf{B}_1 = 0. \quad (6)$$

To analyze an electromagnetic problem, we essentially have to solve the complete system of Maxwell's equations, with appropriate boundary conditions, for a given excitation. Some solution techniques directly solve the differential equations, while others first relate the fields to the field sources (currents and charges), leading to integral equations. For the latter case, solution is facilitated if the electric and magnetic fields are expressed in terms of the electric scalar-potential ( $V$ ) and the magnetic vector-potential ( $\mathbf{A}$ ),

$$\mathbf{E} = -\frac{\partial \mathbf{A}}{\partial t} - \text{grad } V, \quad \mathbf{B} = \text{curl } \mathbf{A}. \quad (7)$$

These potentials are related to the field sources in a simpler form than the fields themselves. There exist various definitions for the potentials. For the numerical analysis of antennas by the method of moments, the Lorentz potentials are predominantly used. They are related by the Lorentz gauge,

$$\text{div } \mathbf{A} = -\frac{\partial V}{\partial t}. \quad (8)$$

The Lorentz potentials are elaborated in Section 2.3.

For completeness, we note that the density of the power flow in an electromagnetic field (i.e., the Poynting vector) is given by

$$\mathbf{P} = \mathbf{E} \times \mathbf{H}. \quad (9)$$

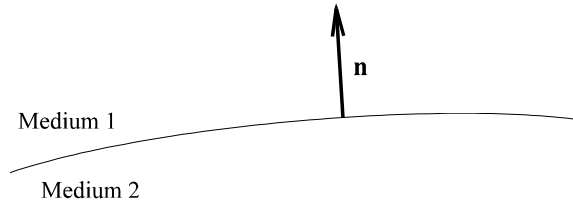


Figure 1. Interface between two media.

## 2.2. Phasor representation and equations in complex domain

In principle, the field vectors can be arbitrary functions of time. For engineering applications (e.g., narrowband signals), it is often sufficient to assume a steady-state (sinusoidal) regime. In this chapter we consider only such a regime.

Before going on, we define complex vectors, as they are essential for the analysis. We shall reveal the canonical form of a sinusoidal scalar quantity on the example of a current that is a sinusoidal function of time. This form reads

$$i(t) = I_m \cos(\omega t + \psi), \quad (10)$$

where  $i(t)$  is the instantaneous current,  $I_m = I_{\text{rms}}\sqrt{2}$  its amplitude (peak value),  $I_{\text{rms}}$  the root-mean-square (rms, or effective) value,  $\omega$  is the angular frequency ( $\omega = 2\pi f$ , where  $f$  is the frequency), and  $\psi$  is the initial phase. The standard procedure in the analysis of sinusoidal regimes is to switch to the domain of the complex frequency, as differential equations in the time domain are converted to ordinary algebraic equations. More precisely, the derivative with respect to time is replaced in the complex domain by the multiplication by  $j\omega$ , which significantly facilitates the analysis.

The complex-domain counterpart of the current  $i(t)$ , i.e., the phasor current,  $I$ , is introduced in two ways. The first one (commonly used, for example, in Europe) is by the equation

$$i(t) = \text{Re}(\sqrt{2}Ie^{j\omega t}), \quad (11)$$

where  $\text{Re}$  denotes the real part, and  $j$  is the imaginary unit ( $j = \sqrt{-1}$ ). The phasor  $I$  is referred to as the complex root-mean-square (rms) or effective value, because  $|I|$  equals the rms value of the current  $i(t)$ . Another possibility (commonly used, for example, in the USA) is

$$i(t) = \text{Re}(Ie^{j\omega t}), \quad (12)$$

in which case  $I$  is referred to as the complex amplitude, because  $|I|$  now equals the amplitude of the current  $i(t)$ . The choice of one of the above definitions does not affect any of the equations in the following sections that are linear relations between complex representatives. However, it does affect relations for power, as well as relations

between the complex numbers and the quantities in the time domain that these complex numbers represent. We assume definition (11), but we shall point out to equations in this chapter that differ depending on the choice of equations (11) or (12).

A sinusoidal time-domain vector, like, for example, the electric-field vector,  $\mathbf{E}(t)$ , is defined in the following way. It is a vector separable into three orthogonal (e.g., Cartesian) components,

$$\mathbf{E}(t) = E_x(t)\mathbf{u}_x + E_y(t)\mathbf{u}_y + E_z(t)\mathbf{u}_z, \quad (13)$$

where each component is a sinusoidal function of time,

$$\left. \begin{aligned} E_x(t) &= E_{xm} \cos(\omega t + \theta_x) \\ E_y(t) &= E_{ym} \cos(\omega t + \theta_y) \\ E_z(t) &= E_{zm} \cos(\omega t + \theta_z) \end{aligned} \right\}, \quad (14)$$

having arbitrary amplitudes ( $E_{xm}$ ,  $E_{ym}$ ,  $E_{zm}$ ) and initial phases ( $\theta_x$ ,  $\theta_y$ ,  $\theta_z$ ), but the same angular frequency ( $\omega$ ). The complex (phasor) electric-field vector,  $\mathbf{E}$ , is obtained by finding complex representatives of  $E_x(t)$ ,  $E_y(t)$ , and  $E_z(t)$ , according to equations (11) or (12), denoted by  $E_x$ ,  $E_y$ , and  $E_z$ , respectively. These phasors are then used as components of the resulting phasor vector,

$$\mathbf{E} = E_x\mathbf{u}_x + E_y\mathbf{u}_y + E_z\mathbf{u}_z. \quad (15)$$

We shall not introduce separate notations for field vectors in the time domain and in the frequency domain. This should not make confusion, as in this chapter we practically do not deal with the vectors in the time domain.

A sinusoidal vector in the time domain is, generally, elliptically polarized. Hence, both its magnitude and direction vary as a function of time. The tip of the vector describes an ellipse. As special cases, the vector can be linearly polarized, when it has a constant direction, but changes the magnitude and sense, or circularly polarized, when it has a constant magnitude, but rotates at a uniform speed. The complex vector, however, does not have a physically defined direction, except for linearly polarized fields. If definition (11) is used, the magnitude of the phasor electric field,  $|\mathbf{E}|$ , has a clear meaning: it is the rms of  $|\mathbf{E}(t)|$ .

Maxwell's equations in the complex domain can be written only for linear media, as the sinusoidal regime can not exist in nonlinear media. Equations (1), (4), (7), and (8) become, respectively,

$$\text{curl } \mathbf{E} = -j\omega\mathbf{B}, \quad \text{curl } \mathbf{H} = \mathbf{J} + j\omega\mathbf{D}, \quad \text{div } \mathbf{D} = \rho, \quad \text{div } \mathbf{B} = 0, \quad (16)$$

$$\text{div } \mathbf{J} = -j\omega\rho, \quad (17)$$

$$\mathbf{E} = -j\omega\mathbf{A} - \text{grad } V, \quad \mathbf{B} = \text{curl } \mathbf{A}, \quad (18)$$

$$\text{div } \mathbf{A} = -j\omega V, \quad (19)$$

where all quantities depend only on the position-vector,  $\mathbf{r}$ . Equations (3) are still formally valid, but all quantities should now be interpreted as being phasors (i.e., in the frequency domain).

If definition (11) is used, the complex Poynting vector is

$$\mathbf{P} = \mathbf{E} \times \mathbf{H}^*, \quad (20)$$

where the asterisk denotes complex conjugate. If definition (12) is used, the complex Poynting vector is

$$\mathbf{P} = \frac{1}{2} \mathbf{E} \times \mathbf{H}^*. \quad (21)$$

### 2.3. Lorentz potentials and Green's function

In a linear homogeneous lossless medium, the electric and magnetic fields can be expressed in terms of the field sources (currents and charges) through the Lorentz potentials, starting from equations (18). Referring to Figure 2, the potentials are related to the field sources as

$$\mathbf{A}(\mathbf{r}) = \mu \int_{v'} \mathbf{J}(\mathbf{r}') g(\mathbf{r}, \mathbf{r}') dv', \quad V(\mathbf{r}) = \frac{1}{\epsilon} \int_{v'} \rho(\mathbf{r}') g(\mathbf{r}, \mathbf{r}') dv', \quad (22)$$

where  $\mathbf{r}$  is the coordinate of the field point M (i.e., the point at which the potentials and fields are evaluated),  $v'$  the volume occupied by the sources,  $\mathbf{r}'$  the coordinate of the source point (i.e., the point at which the field source element  $dv'$  is located),

$$g(\mathbf{r}, \mathbf{r}') = \frac{\exp(-jk|\mathbf{r} - \mathbf{r}'|)}{4\pi|\mathbf{r} - \mathbf{r}'|} \quad (23)$$

is Green's function, and  $k = \omega\sqrt{\epsilon\mu}$  is the phase coefficient. Losses in media can be incorporated in the above equations by taking the permittivity and permeability to be complex. Note that Green's function is, generally, the response to an impulse function (Dirac's delta function). Here it gives the potential due to a point source, which can be regarded as a spatial delta function.

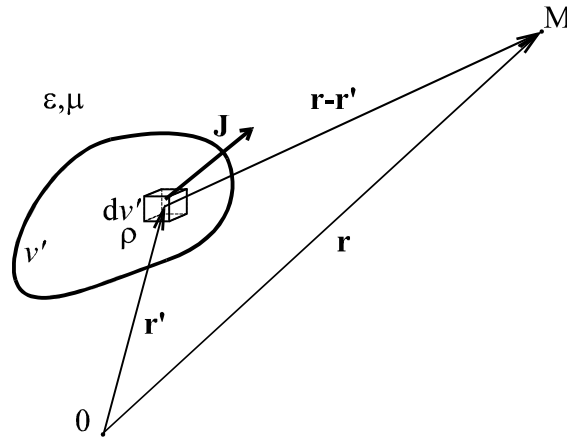


Figure 2. Coordinate system for evaluation of potentials.

Equations (22) are written assuming currents and charges distributed throughout the source volume,  $v'$ . In many cases the currents and charges can be assumed distributed over surfaces, like charges on conducting bodies in electrostatics, or currents and charges on metallic bodies when the skin effect is fully pronounced. It is also possible to have the sources practically distributed along lines (filaments), like currents and charges on thin-wire conductors. For surface sources equation (22) is to be modified appropriately by taking the densities of the surface currents ( $\mathbf{J}_s$ ) and charges ( $\rho_s$ ), and integrating over the source surface ( $S'$ ), i.e.,

$$\mathbf{A}(\mathbf{r}) = \mu \int_{S'} \mathbf{J}_s(\mathbf{r}') g(\mathbf{r}, \mathbf{r}') dS', \quad V(\mathbf{r}) = \frac{1}{\epsilon} \int_{S'} \rho_s(\mathbf{r}') g(\mathbf{r}, \mathbf{r}') dS'. \quad (24)$$

For filamental currents and charges the current intensity ( $I$ ) and the per-unit-length charge density ( $\rho_l$ ) should be used, and integrated along the source line ( $L'$ ), yielding

$$\mathbf{A}(\mathbf{r}) = \mu \int_{L'} \mathbf{u}(\mathbf{r}') I(\mathbf{r}') g(\mathbf{r}, \mathbf{r}') dl', \quad V(\mathbf{r}) = \frac{1}{\epsilon} \int_{L'} \rho_l(\mathbf{r}') g(\mathbf{r}, \mathbf{r}') dl', \quad (25)$$

where  $\mathbf{u}$  is the unit vector tangential to the line. For surface and line sources the continuity equation (17) is replaced by

$$\text{div}_s \mathbf{J}_s = -j\omega\rho_s, \quad (26)$$

$$\frac{dI}{ds} = -j\omega\rho_l, \quad (27)$$

respectively, where the surface divergence ( $\text{div}_s$ ) in equation (26) implies differentiation only with respect to two local coordinates on the surface, and  $s$  in equation (27) is a local coordinate along the line.

To simplify the analysis, it is convenient to relate the fields only to the currents, thus avoiding dealing with the charges. There are two basic possibilities to express the fields in terms of only the current density. The first way is to combine equations (18) with the Lorentz gauge in the complex domain, (19). As the result, the electric field is expressed only in terms of the magnetic vector-potential as

$$\mathbf{E} = -j\omega\left(\mathbf{A} + \frac{1}{k^2}\text{grad div } \mathbf{A}\right). \quad (28)$$

Using equation (28) and the first equation in (22), the electric field is related only to the currents. The second way is to express the charge density from the continuity equation (17) in terms of the current density, substituting into the second equation in (22), and then using (18).

For 3D static problems (including electrostatics), Green's function (23) reduces to

$$g(\mathbf{r}, \mathbf{r}') = \frac{1}{4\pi|\mathbf{r} - \mathbf{r}'|}. \quad (29)$$

For 2D high-frequency problems, Green's function is

$$g(\mathbf{r}, \mathbf{r}') = -\frac{j}{4}H_0^{(2)}(k|\mathbf{r} - \mathbf{r}'|), \quad (30)$$

where  $H_0^{(2)}(x)$  is Hankel's function of the second kind and order 0. In this case, Green's function gives the potential of a uniform, infinitely long line source, which is the elemental source in 2D problems. For low frequencies, Green's function (30) can be approximated by

$$H_0^{(2)}(k|\mathbf{r} - \mathbf{r}'|) \approx 1 - j\frac{2}{\pi}\log\frac{\gamma k|\mathbf{r} - \mathbf{r}'|}{2}, \quad (31)$$

where  $\gamma = 1.781\dots$  is Euler's constant, yielding

$$g(\mathbf{r}, \mathbf{r}') \approx -\frac{j}{4} - \frac{1}{2\pi}\log\frac{\gamma k|\mathbf{r} - \mathbf{r}'|}{2}. \quad (32)$$

As frequency diminishes, tending towards the static case, Green's function (32) can be substituted by

$$g(\mathbf{r}, \mathbf{r}') = -\frac{1}{2\pi}\log|\mathbf{r} - \mathbf{r}'| \quad (33)$$

under the condition that the integral of the field sources (e.g., the total charge of the system) is zero. If this condition is violated, the static potentials resulting from equation (32) become infinitely large.

Only very few electromagnetic field problems have analytical solutions. Most such solutions can be found in reference [16]. Examples of analytically solvable problems in electrostatics are a conducting sphere and an infinite conducting circular cylinder. Among high-frequency problems, analytical solutions exist for the propagation of uniform plane waves, and for the wave propagation along certain transmission lines (e.g., coaxial lines) and waveguides (rectangular and circular waveguides), but there are no analytical solutions for antennas. Note that the well-known sinusoidal current distribution along a thin wire [1] is only an approximation, the better the thinner the antenna conductor. Most problems that have closed-form solutions are impractical because realistic structures often have complicated shapes, but they can serve as an estimate of properties of the realistic structures. For example, the capacitance of an arbitrarily shaped conductor is larger than the capacitance of the largest inscribed sphere, but smaller than the capacitance of the smallest circumscribed sphere.

The only available way to precisely analyze practical structures is to implement numerical techniques. The method of moments is one of them, particularly suitable for structures that are not too large in terms of the wavelength. The limits depend on the complexity of the structure analyzed, numerical implementation, and

computer resources. As estimation of the order of magnitude, the MoM can commonly handle wire structures that are 1000 wavelengths long, and surfaces whose area is 100 square wavelengths.

### 3. Method of moments

#### 3.1. Linear operator equations

As stated in Section 1, numerical solutions of electromagnetic field problems are usually classified into two groups. The first one attacks directly electromagnetic fields, and the second one attacks the field sources. In both cases, the equations that are to be solved are linear operator equations in terms of the unknowns (the fields, viz. the sources). However, in the first case the equations are differential, whereas in the second case they are integral. Both classes of equations belong to the general class of linear operator equations, which have the common form

$$L(f) = g, \quad (34)$$

where  $L$  is the operator,  $g$  is the source or excitation, which is assumed to be a known function, and  $f$  is the field or response, which is the unknown function to be determined. The linearity of the operator follows from the linearity of Maxwell's equations and the constitutive equations, as we consider only linear media. We assume there exists a unique solution to equation (34).

For the first group of numerical methods  $L$  is a differential operator. It generally involves derivatives with respect to three spatial coordinates. For the time-domain analysis, derivatives with respect to time are also involved. Further,  $f$  is a field vector or potential (depending on the formulation), whereas  $g$  is a known quantity, e.g., the field or potential due to an incident wave. For the second group of numerical methods  $L$  is an integral operator,  $f$  represents the field sources, and  $g$  is, again, a known quantity that models the excitation.

Irrespective of the approach, the operator equation (34) can be solved following the numerical procedure known under the generic name of the method of moments (MoM), which is a general technique for solving linear operator equations.

#### 3.2. Basic steps of the method of moments

The basic idea of the MoM is as follows. The unknown quantity ( $f$ ) is expanded in terms of a set of linearly independent known functions,  $f_n$  (referred to as basis or expansion functions), i.e., it is approximated by the following finite series:

$$f \approx \sum_{n=1}^N \alpha_n f_n, \quad (35)$$

where  $\alpha_n$  are unknown coefficients yet to be determined. The expansion functions should be chosen, usually based on experience, so that reasonable approximation of  $f$  is obtained with a small number of terms,  $N$ .

When equation (35) is substituted into (34), one obtains the approximate equation

$$L\left(\sum_{n=1}^N \alpha_n f_n\right) \approx g. \quad (36)$$

Due to the linearity of the operator, we can rewrite equation (36) as

$$\sum_{n=1}^N \alpha_n L(f_n) \approx g. \quad (37)$$

Note that equation (37) can not be exactly satisfied at all points, as we have a finite number of terms in the series. Exceptions are rare examples that do have analytical solutions, but which are not of our interest here. The unknown coefficients ( $\alpha_n$ ) should now be determined such that equation (37) is satisfied in a sense. Hence, a measure is needed describing the degree of accuracy to which the left side and the right side of equation (37) match.

In the MoM, this measure is obtained in the following way. Both sides of equation (37) are multiplied by a known, properly selected function, referred to as the weighting function,  $w_m$ , and the results integrated over a spatial region. This integration is a special, but very frequent case of an inner product of two functions,  $f$  and  $g$ , which is denoted by  $\langle f, g \rangle$ . Generally, the inner product of elements  $f$  and  $g$  of a given space is a scalar, which satisfies the following conditions:  $\langle f, g \rangle = \langle g, f \rangle$ ,  $\langle \alpha f + \beta g, h \rangle = \alpha \langle f, h \rangle + \beta \langle g, h \rangle$ ,  $\langle f, f^* \rangle > 0$  if  $f \neq 0$ , and  $\langle f, f^* \rangle = 0$  if  $f = 0$ , where  $\alpha$  and  $\beta$  are arbitrary scalars, and  $h$  is another element of the same space.

The choice of the weighting functions and the inner product is, again, based on experience. Now we have

$$\sum_{n=1}^N \alpha_n \langle w_m, L(f_n) \rangle = \langle w_m, g \rangle. \quad (38)$$

The inner products in equation (38) are definite numbers, as they can be evaluated analytically or, more frequently, numerically. Hence, equation (38) represents a linear equation in coefficients  $\alpha_n$ . To obtain a determined system of linear equations for these coefficients, the weighting procedure is done for a linearly independent set of  $N$  functions, yielding

$$\sum_{n=1}^N \alpha_n \langle w_m, L(f_n) \rangle = \langle w_m, g \rangle, \quad m = 1, \dots, N. \quad (39)$$

Equation (39) represents a system of  $N$  ordinary linear equations in  $N$  unknowns, and it can be solved using various techniques. As a rule, the methods based on differential equations result in huge, but sparse systems of linear equations, which are solved using specific techniques. The methods based on integral equations result in more compact, but full systems, which are usually solved using the Gaussian elimination or similar techniques [17], like the LU decomposition. Note that the classical matrix inversion is an inefficient approach, as it requires about three times more operations, and thus three times longer CPU time, than the Gaussian elimination. Large full MoM systems of linear equations have also been successfully solved using other techniques, such as the conjugate gradients [18] alone or in combination with the fast Fourier transform [19].

To prepare a computer code that uses the MoM to solve a complex electromagnetic field problem, usually requires a lot of work and experience. Often, codes are specialized for certain classes of problems. There is no guarantee of convergence, and in most cases there does not exist a useful measure of accuracy of the solution obtained. In spite of all these deficiencies, the MoM is the most powerful tool available nowadays for analysis of fairly general electromagnetic field problems that involve linear media.

The expansion and testing functions can be arbitrary. However, to provide an efficient solution, the expansion functions should be selected such that the solution can be well approximated by a relatively small number of functions. Similarly, the weighting functions should provide a reliable measure of discrepancy between the two sides of equation (37). On the other hand, all these functions should be selected bearing in mind complexity and speed of computations, and flexibility to accommodate to a wide range of problems [20].

Expansion and testing functions may coincide, i.e., we can take  $f_n = w_n$ ,  $n = 1, \dots, N$ . In this case we have a Galerkin solution, which is equivalent to the Rayleigh-Ritz variational method, often used in the finite-element approach.

In the literature there is a certain confusion between the terms "method of moments" (MoM) and "finite-element method" (FEM), emerging from the existence of two distinct groups of practitioners. One group usually deals with integral equations and solves them using the MoM, thus identifying the MoM with the solution of integral equations. The other group usually deals with differential equations and solves them also using the MoM, but with subsectional basis functions referred to as finite elements, thus identifying the FEM with the solution of differential equations. This second group also claims that solving integral equations with subsectional basis functions is an application of the FEM. To add to the confusion, in the FEM, the starting differential equation that is to be solved is often formulated from the variational (energy) principle, thus obscuring the fact that the same result can be obtained if the Galerkin procedure is directly applied to a differential equation derivable from Maxwell's equation. The truth seems to be that both groups essentially do similar things, but they speak somewhat different languages. In this chapter we predominantly solve integral equations using the MoM, so there should be no confusion about the terms.

Both expansion and testing functions can be divided into two categories. The first category is subdomain functions. The domain, where the unknown function ( $f$ ) is defined, is divided into a number of small subdomains. Each basis function is defined only on one subdomain (i.e., it is assumed zero elsewhere), and it is a very simple function. Such a choice simplifies evaluation of matrix elements, and it can relatively easily accommodate an arbitrary geometry. However, it may result in instabilities as the approximation of the unknown function is

discontinuous or has discontinuous derivatives, and it may require a large number of basis functions for an accurate solution.

The simplest subdomain approximation is using samples (impulses, Dirac's delta functions). This procedure is seldom used for expansion in the MoM, except with the finite-difference method. If used, it may require modifying the original operator to better suit the expansion. For example, instead of the derivative, a finite-difference scheme is used. However, impulses are often used as testing functions, i.e.,  $w_m = \delta_m(P_m)$ , where  $\delta_m(P_m)$  denotes an impulse centered at a point  $P_m$ , amounting to the point-matching (collocation) technique. In this approach, the integration of the product of a function with the impulse, involved in the inner product, yields simply the value of the function at the center of the impulse,  $P_m$ , i.e.,  $\langle w_m, g \rangle = g(P_m)$ , and (38) can be interpreted as equating (matching) the values of the left and right sides at this point. Thus, equation (39) is interpreted as requiring (37) to be simultaneously satisfied at  $N$  discrete points,  $P_m$ ,  $m=1, \dots, N$ , referred to as matching points. The point-matching method simplifies evaluation of the matrix elements as the integration involved in the inner product is avoided. It annihilates the error in the operator equation at matching points, but there is no guarantee about the behavior of the error elsewhere, between adjacent matching points.

Slightly more complicated are pulse functions. When used for expansion, they yield a staircase (piecewise-constant) approximation of  $f$ . A pulse is defined analytically as

$$f_n = \begin{cases} 1 & \text{in subdomain } n \\ 0 & \text{elsewhere} \end{cases} \quad (40)$$

Figure 3a shows a set of pulse expansion functions in one dimension and the resulting staircase approximation.

The piecewise-constant approximation is discontinuous. A better approximation is the piecewise-linear (triangular, rooftop) approximation, which is continuous, but has a discontinuous first derivative. Analytically, this approximation can be constructed in two ways. For simplicity, we consider an one-dimensional expansion. The first way is assuming a linear function on a subdomain, and then matching the approximations on adjacent subdomains to obtain continuity. Alternatively, a subdomain function can be assumed a triangle, each triangle defined on two adjacent subdomains. Hence, the triangles partially overlap, as shown in Figure 3b.

More sophisticated functions can be designed using more complicated subdomain functions and introducing additional constraints. Examples are spline approximations and functions that include edge effects. The edge effect is pronounced, for example, on sharp edges and wedges of perfectly conducting bodies, where the current and charge densities tend to infinity, but are integrable. An expansion function that closely resembles such source distributions may expedite the numerical solution.

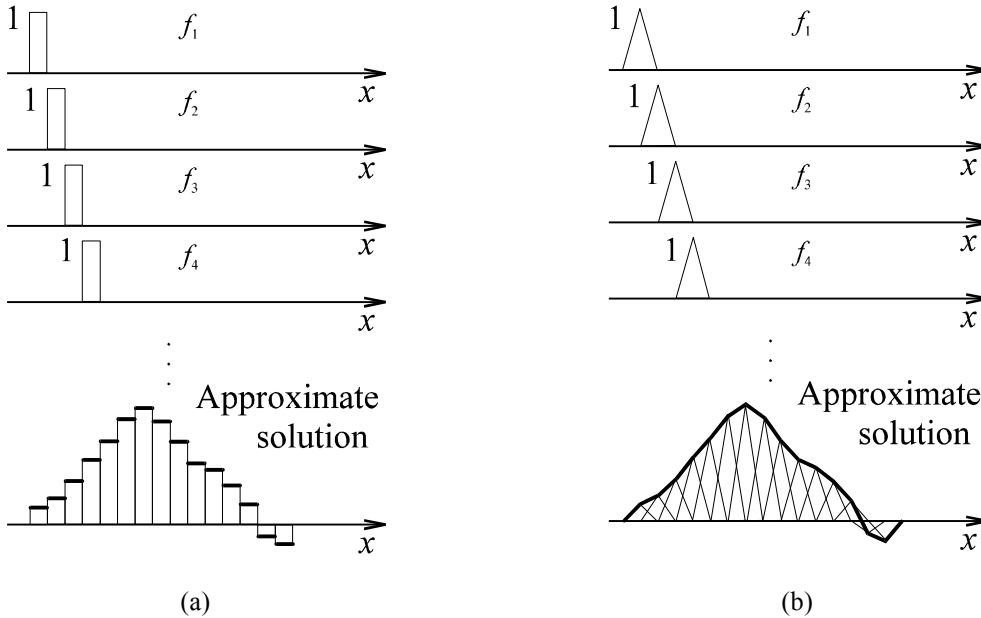


Figure 3. Subdomain approximations: (a) piecewise-constant, and (b) piecewise-linear.

The approximation by expansion functions involved in the MoM means not only an approximation of the unknown function, but also of the geometry of the problem analyzed. The approximation of the geometry means a modification of the shape of the domain where the unknown function is defined, as the subdomains may not exactly match the shape of the domain. As an example, let us consider a conducting body in electrostatics, which is analyzed using an integral equation for its surface charges (Figure 4). We assume the pulse approximation to be implemented.

A pulse can be defined on a simple surface (usually a triangle or a quadrilateral) that is often referred to as a patch. In this case, pulses are two-dimensional functions. Hence, the original surface is approximated by a set of patches. Obviously, the approximate charges are distributed over a different surface than the original surface of the conducting body. To minimize the error introduced by the geometry approximation, it is usually advisable to make the new (approximating) surface "oscillate" around the original surface.

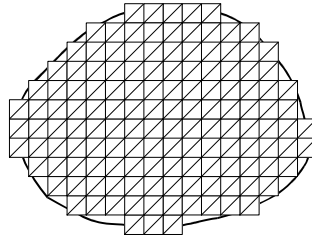


Figure 4. Surface patches associated with the pulse approximation of the surface charges of a conducting body in electrostatics.

The second category of expansion and testing functions is entire-domain functions. Each function is defined on the entire domain of interest, so that all functions are non-zero on the whole domain. An example is power functions ( $1, x, x^2, x^3, \dots$ ) which, when combined into equation (35), yield a polynomial approximation [21,22]. Another example is a set of trigonometric functions, amounting to the Fourier expansion. Sometimes rational functions are used, or functions that involve special effects, like the asymptotic charge and current distribution behavior near edges or wedges.

In practice, however, the entire domain is divided into a small number of relatively large subdomains. For example, a wire Yagi-Uda antenna is divided into its physical segments, i.e., dipoles. The expansion and testing functions are then defined on these large subdomains. This procedure is referred to as the almost-entire-domain approximation.

In the numerical implementation of the entire-domain or almost-entire-domain approximations, a complicated evaluation of matrix elements is often encountered, requiring high-precision computations. This kind of functions may well accommodate complex geometries and yield good results with a smaller number of unknowns and in a substantially shorter CPU time than the subdomain functions. However, the technique is prone to instabilities with increasing the order of approximation due to an ill-conditioned system of linear equations (39).

The more complicated the basis functions, the more analytical preparation is usually required before starting to write the computer code. A set of basis functions is usually suitable for a certain class of problems, but not for a general structure. Hence, a code customized for a class of problems is usually more efficient than a general code.

Convergence of the MoM solution can not be guaranteed in most cases. At first, results usually improve with increasing the number of unknowns, but then they suddenly diverge. This is caused by various problems: approximations involved in the starting equation that is solved, inadequacy of the basis functions, insufficient accuracy of computing the basic integrals, propagation of numerical errors when solving the system of linear equations, etc.

### 3.3. Formulation of integral equations

We restrict our attention here to the MoM applications to solving integral equations, where the unknowns are field sources (currents and charges). These integral equations are, generally, formulated in the following three steps.

The first step is to enforce a boundary condition from (5) or (6) for the electric or magnetic field, or utilize a constitutive relation from (3). For example, if we analyze a body made of a perfect conductor (a PEC body), the tangential component of the electric field on its surface is zero.

The second step is to express the fields in terms of the potentials, according to (18) or (28), and plug into the boundary condition or constitutive relation, as appropriate.

The third step is to express the potentials in terms of the sources, according to (22). Instead of equations (22), equations (24) should be taken for surface sources, and (25) for filamental sources. Upon a substitution into the equation derived in the second step, we finally obtain the integral equation for the unknown field sources.

There is a variety of equations that can be formulated in this way. A given, particular problem can usually be solved using several equations. Depending on the field involved in the first step (the electric field or the magnetic field), the integral equations are, generally, categorized as electric-field integral equations (EFIE) and magnetic-field integral equations (MFIE). There are some cases when the two fields are involved simultaneously, resulting in combined-field integral equations.

### 3.4. Example

To illustrate the basic MoM concepts, we consider an example of a conducting body in an electrostatic field in a vacuum (Figure 5). The body is equipotential, its potential is a constant,  $V_0$ , and the tangential component of the electric field at its surface ( $S$ ) is zero. Hence, there are two approaches to start with: imposing the boundary condition for the potential,  $V_0 = \text{const}$  on the body surface, and imposing the condition for the electric field, i.e., the first of equations (6). Theoretically, both approaches should have the same answer, but there are differences in the numerical implementation in the two cases. We adopt the first approach, as the kernel of the resulting integral equation is simpler and easier for evaluation.

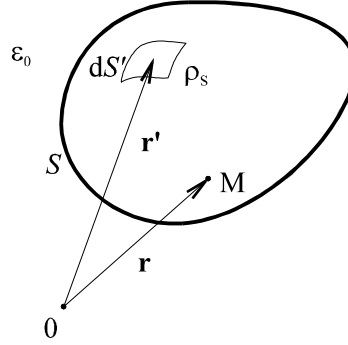


Figure 5. Coordinate system for setting up an integral equation for a charged conducting body in electrostatics.

We take a field point  $M(\mathbf{r})$  at the conductor surface (Figure 5). The boundary condition is simply  $V = V_0$  for any such point. The unknown is the distribution of conductor surface charges ( $\rho_s$ ), and the potential is expressed in terms of these charges using (24) and (29). The resulting integral equation reads:

$$\frac{1}{\epsilon_0} \int_S \rho_s(\mathbf{r}') g(\mathbf{r}, \mathbf{r}') dS' = V_0 \quad \text{for arbitrary } \mathbf{r} \text{ on } S. \quad (41)$$

Note that the source surface and the field surface coincide in this case, i.e., the body surface is both  $S$  and  $S'$ .

Assume, now, the conducting body is a cylindrical rod, as shown in Figure 6. Although we consider an electrostatic example, the cylindrical rod will lead us to certain conclusions important in the analysis of wire antennas. Let the rod length be  $L$  and radius  $R$ . Let us compute the capacitance of the rod.

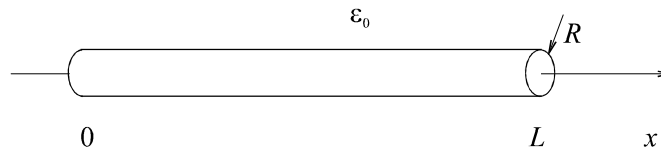


Figure 6. A conducting rod in electrostatics.

The integration over  $S'$  in (41) means a double integral: one integration along the  $x$ -coordinate, and another along the circumferential coordinate, e.g., the azimuthal angle  $\phi$ , around the rod. Due to symmetry,  $\rho_s$  is a function of  $x$  alone, i.e., the unknown charge distribution does not depend on  $\phi$ . However, the resulting double integral is still hard for evaluation (regardless of the basis functions used) as it has a singularity when  $\mathbf{r}'$  approaches  $\mathbf{r}$ . One integration can be carried out explicitly, but the second integration can be carried out only numerically, still with significant difficulties associated with singularities.

A simplification of (41) for this case can be made using the concept of the extended boundary conditions [23]. The rod is assumed to be a solid conducting body. Hence, in electrostatics, its potential is  $V_0$  not only on the surface, but also at any point of its interior. In particular, we have  $V = V_0$  at any point on the  $x$  axis for  $0 \leq x \leq L$ . Alternatively speaking,  $E_x = 0$  for  $0 < x < L$ . According to this concept, instead of imposing a boundary condition on the surface of the body, we impose a condition at some points at the body interior. There are certain restrictions where the extended boundary conditions are to be imposed to obtain a numerically stable solution, but we can not discuss this question here. For simplicity, we impose that along the  $x$  axis  $V = V_0$ , which reduces equation (41) to

$$\frac{1}{\epsilon_0} \int_{x'=0}^L \rho_l(x') g(x, x') dx' = V_0 \quad \text{for } 0 \leq x \leq L, \quad (42)$$

where  $\rho_l(x') = 2\pi R\rho_s(x')$  is the per-unit-length charge density and  $g(x, x') = \frac{1}{4\pi\sqrt{(x-x')^2 + R^2}}$  is the kernel of

the integral equation. Note that  $x$  and  $x'$  are measured along the same coordinate line. In equation (42) we have only a single integral (over  $x'$ ). An identical result would be obtained if the surface charges of the rod were located along a filament on the surface generatrix, i.e., if they constituted a line charge.

Note, however, that the integral equation (42) has a trouble spot. At  $x = 0$  and  $x = L$ , in reality, there are two charged circular surfaces (disks, i.e., the end-caps), which are not encompassed by equation (42). In other words, we have neglected the charges on the two discs closing the rod. We impose the potential to be constant along the axis of the rod. However, this condition can not be satisfied exactly without taking into account the effect of the caps [21]. As a consequence, equation (42) gives diverging results when a very high order approximation for the charge distribution is taken.

An alternative interpretation of equation (42) can be made in terms of the equivalent sources [24]. We observe the boundary conditions on the surface of the rod. However, instead of considering the original sources, i.e., the charges located on the surface of the rod, we consider some equivalent sources encapsulated by  $S$ . There are certain rules where the equivalent sources should be located to obtain a numerically stable solution, but we can not discuss this question here. Equation (42) amounts to assuming the equivalent sources to be a nonuniform line charge, of the per-unit length density  $\rho_l(x')$ , located on the  $x$  axis for  $0 \leq x' \leq L$ .

Regardless of interpretation, equation (42) is simpler than (41) as the dimensionality of the mathematical problem is reduced by one. Such an approach is not only used in electrostatics; it is almost always implemented in the analysis of wire antennas and scatterers [21,25], with the dynamic Green's function (23), when it is referred to as the thin-wire approximation.

Once we have formulated the integral equation, (42), we shall solve it by the MoM. We adopt a simple procedure: the pulse approximation for the unknown charge distribution as a function of  $x'$  and the point-matching testing. For the approximation, we take  $N$  uniform pulses along the  $x$  axis. The choice of the approximation functions is arbitrary, and the selection here is targeted for simplicity. The choice of the uniform pulse distribution is not the most efficient one. For example, taking nonuniform pulses, shorter towards the ends of the rod, would yield a more efficient solution.

For the uniform pulse distribution the length of each pulse is  $\Delta x = L/N$ . The  $n$ th pulse, belonging to the  $n$ th subdomain, is located on  $x' \in [(n-1)\Delta x, n\Delta x]$ , where  $n=1, \dots, N$ . The matching points are assumed to be located at the subdomain midpoints, i.e., at  $x_m = (m-0.5)\Delta x$ ,  $m=1, \dots, N$ , which is, from experience, a good policy, although not the only possibility. This choice of the expansion and testing functions reduces equation (42) to the following system of linear equations:

$$\frac{1}{4\pi\epsilon_0} \sum_{n=1}^N \alpha_n \int_{x'=(n-1)\Delta x}^{n\Delta x} \frac{1}{\sqrt{(x_m - x')^2 + R^2}} dx' = V_0, \quad m=1, \dots, N. \quad (43)$$

We can arbitrarily adopt  $V_0 = 1$  V (as this choice does not affect the capacitance). The integral in equation (43) can be evaluated analytically using

$$\int_{x'=x_1}^{x_2} \frac{1}{\sqrt{(x_m - x')^2 + R^2}} dx' = \log \frac{x_2 - x_m + \sqrt{(x_m - x_2)^2 + R^2}}{x_1 - x_m + \sqrt{(x_m - x_1)^2 + R^2}}. \quad (44)$$

Note that equation (44) may lead to numerical difficulties when  $R$  is small compared with  $|x_m - x_1|$  for  $x_1 - x_m < 0$ , or with  $|x_m - x_2|$  for  $x_2 - x_m < 0$ . The remedy is to rationalize the denominator, viz. numerator, as appropriate.

Once the system of linear equations (43) is solved, we obtain the approximate charge distribution. The capacitance of the rod can then be evaluated as

$$C = \frac{\sum_{n=1}^N \alpha_n \Delta x}{V_0}. \quad (45)$$

As a numerical example, we take  $L = 1$  m and three different rod radii,  $R = 1$  mm,  $R = 10$  mm, and  $R = 100$  mm. Linking these data to wire antennas, the first radius corresponds to a thin wire, and the third radius to a thick wire. The classification is based on the ratio of the cylinder length to its diameter.

Table 1 shows the rod capacitance as a function of the number of pulses ( $N$ ). For all three rods, the results initially converge with increasing  $N$ . However, the capacitance of the thickest rod starts oscillating already for  $N = 64$ . The capacitances of the other two rods also start oscillating, but for much larger  $N$  than shown in Table 1. This break-down is a consequence of neglecting the end effect. The effect is more pronounced if the charge distribution is observed, as it has an erratic behavior in the vicinity of the ends even for low values  $N$ , e.g., for  $N = 64$  for  $R = 10$  mm, and  $N = 8$  for  $R = 100$  mm, when  $\Delta x$  becomes of the order of magnitude of  $R$ .

Table 1. Capacitance ( $C$ ), in pF, of the rod shown in Figure 6, for  $L = 1$  m and three different radii ( $R$ ), versus the number of pulses.

$N$	2	4	8	16	32	64	128	256	512
$R = 1$ mm	8.225	8.331	8.394	8.432	8.456	8.470	8.480	8.487	8.492
$R = 10$ mm	12.469	12.731	12.905	13.026	13.114	13.182	13.237	13.286	13.331
$R = 100$ mm	25.521	26.778	27.764	28.579	29.314	30.017	29.798	30.328	30.273

## 4. Antenna analysis

### 4.1. Introduction

The method of moments is applicable to many antenna types. The analysis can also involve, to a certain extent, the environment where the antenna is located, like a mounting mast, or a stratified ground. The MoM can handle antennas whose dimensions are very small, a fraction of the wavelength, up to about one thousand wavelengths for wire antennas. To have an antenna that radiates efficiently, its dimensions must not be too small: the order of magnitude of  $1/10$  of the operating frequency is considered as a practical minimum. Well-written MoM codes, however, can analyze structures whose dimensions are many orders of magnitude smaller.

The applicability of MoM is limited by the complexity of the antenna, which requires a precise modeling of various antenna parts, and the antenna overall dimensions, as both factors influence the total number of unknowns required to obtain an accurate solution. Depending on computer resources, the number of unknowns is nowadays usually limited to a few tens of thousand, but this limit is pushed higher with the increase of available CPU power and fast memory. For higher frequencies, when the dimensions of the antenna and nearby relevant objects are many wavelengths, other, high-frequency techniques are used, as described in another chapter in this book.

For the present purpose, antennas are classified according to the complexity of their analysis into the following three groups:

- wire antennas,
- surface (metallic) antennas, and
- metallo-dielectric antennas.

The basics of the analysis of each group are presented below.

### 4.2. Wire antennas

#### 4.2.1. Definition of wire antennas

Wire antennas are structures made of wire-like conductors: conductor radii are much smaller than their lengths and the wavelength at the operating frequency (Figure 7). Conductors can be perfect (PEC) or the wires can be loaded (e.g., resistively or inductively). Our primary interest here is PEC structures.

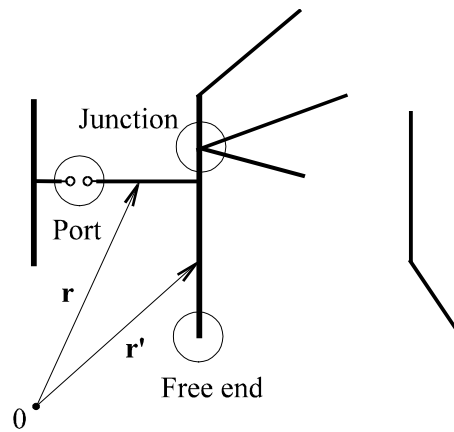


Figure 7. A wire antenna.

Examples of wire antennas are simple wire dipoles, V-antennas, loops and rhombic antennas used for HF communications, tower broadcast antennas for MF and LF bands, Yagi-Uda antennas and log-periodic dipole arrays used in the HF, VHF, and UHF bands, etc. However, the analysis of such structures can be extended to some other antennas and scatterers that can be approximated by wire structures, like aircraft at lower frequencies and some printed-circuit antennas, or whose surfaces can be approximated by wire-grid models. Some structures in the analysis of the electromagnetic compatibility (EMC) and electromagnetic interference (EMI) can be modeled by wires and wire grids. Examples are cages, shields with openings, power lines, etc.

We consider wire structures assembled from one or more straight PEC wires, referred to as segments, each having a circular cross section of a constant radius, arbitrarily oriented and interconnected. A generalization towards curved wire segments and wires with varying radii is straightforward, but not always easy for implementation. Alternatively, a curved segment or a segment with a varying radius can be approximated by a chain of straight segments, of uniform cross sections.

The segments can also have concentrated or distributed loadings, but we shall not present the corresponding analysis due to the lack of space. A further possibility is to approximate a conductor of an arbitrary cross section by an equivalent wire of a circular cross section, by using the concept of equivalent radius [26], as well as approximate a printed-circuit trace on a substrate (usually without a ground plane) or a dielectric-coated wire by an equivalent wire of a circular cross section and a series distributed inductive loading.

The wire segments can be isolated in space or placed near an object, such as above a perfectly conducting ground plane. In the presence of certain objects of well-defined shapes, the antenna analysis using the MoM can be carried out by modifying Green's functions, instead of treating the object itself by the MoM approach. For example, the influence of a PEC ground plane is substituted by the antenna image and Green's function contains two terms of the form (23) – one for the original, and another for the image. Another example is an antenna placed above or in a stratified medium, in which case Sommerfeld's theory is applicable [27], which is beyond our scope here.

The wire structure can be driven at one or more ports or excited by a plane wave of an arbitrary polarization. We are interested in evaluating the current distribution along antenna conductors, near and far fields, port impedance, admittance, and scattering parameters, etc. The primary goal is to evaluate the distribution of the currents and charges along the wires. Other quantities of interest can thereafter be found by postprocessing. The current distribution can be evaluated only numerically and the MoM is the key tool that has been used for decades for this purpose. Generally, the analysis can be carried out in the frequency domain (steady state), or in the time domain (transients). We shall limit our attention here to the frequency-domain analysis.

#### 4.2.2. Integral equations and their solution

For the frequency-domain analysis, various integral and integro-differential equations have been used: Pocklington's equation, two-potential equation, Schelkunoff's equation, and Hallén's equation [21,25,28]. The first three equations are formulated starting from the boundary condition for the electric field, which is the first equation in (6). They differ in the way the electric field is related to the wire currents. In Pocklington's equation, the electric field is expressed only in terms of the magnetic vector-potential, using equation (28). The resulting integral equation involves only the antenna currents, but the kernel of the equation is hard for integration, as it involves the first-order and the second-order derivative of Green's function. The two-potential equation uses the first equation in (18), and the result is an equation where the unknowns are both the current and its first derivative with respect to a local coordinate along the wire axis. The kernel of this equation is easier to handle than in Pocklington's equation. This is the most widely used equation for the analysis of wire antennas and scatterers, and its extension is straightforward to more complicated antenna structures, like surface and metallo-dielectric antennas. Schelkunoff's equation is convenient for parallel wires. It has a mild kernel, but it involves the current and its first two derivatives. Hallén's

equation is most complicated to set up in the general case, as it is formulated for the magnetic vector-potential, not for the electric field. The magnetic vector-potential is solved from this equation, and then it is expressed in terms of the currents. Hallén's equation yields most stable and accurate results, but it is not available for generalization to other antenna structures. Hence, in Section 4.2.3 we focus our attention to the two-potential equation.

In the analysis of wire antennas, the thin-wire approximation is almost always used. As the consequence, we deal with filamental currents (in the direction of the wire axis), and the unknown quantity is the distribution of the current along the axes of the wire segments.

Various approximations (basis functions) are used for the current distribution. Examples of subdomain approximations are the pulse (piecewise-constant) approximation, as, for example, used in [29], triangular (piecewise-linear), and piecewise-sinusoidal approximation [30]. Among almost-entire domain approximations, polynomials [21,22] have been used predominantly, either alone, or in combination with trigonometric functions. The subdomain approximations are easier for computer programming. In particular, the basic integrals encountered in the sinusoidal approximation can be evaluated explicitly. However, the most efficient codes are claimed to be those based on the polynomial approximation (e.g., [31,32]). This may be due to the fact that the subdomain approximations applied to long, smooth wire segments artificially introduce significant discontinuities, which deteriorate the quality of the solution. For example, the pulse approximation for the current (Figure 3a) is discontinuous at subsegment ends, and the associated charge distribution is singular. The electric field produced by such an approximation has large peaks at subsegment boundaries. The piecewise-linear and piecewise-sinusoidal approximations have a continuous current, but a discontinuous charge distribution, also leading to artificial peaks in the electric field, though milder than for the pulse approximation. On the other hand, the almost-entire domain approximations produce a smooth electric field along a wire segment, except in the vicinity of the segment ends. However, in regions where the current distribution suffers rapid variations, such as in the excitation region, it is often necessary to split a physical wire segment into a number of shorter segments to provide a more flexible approximation of the current and charge distributions. Hence, it is a skillful blend of subdomain and entire-domain functions that gives the best results in the general case.

For weighting, the most frequent choices are the point matching procedure [33], pulse weighting functions [29,31], and the Galerkin procedure [34,32]. The point matching procedure is the simplest one. However, it does not properly take care of large fields in the vicinity of antenna discontinuities, like junctions, bends, and excitation regions, except with Hallén's equation, and other measures may be necessary for these regions to provide an accurate solution [31,21]. The pulse weighting functions associated with the two-potential equation enable an explicit integration of the  $-\text{grad } V$  term in equation (18), which leads to numerical simplification [29]. The Galerkin procedure requires most analytical preparation, but it is reported to yield most accurate and stable results [32].

### 4.2.3. Two-potential equation

As an example, we shall outline the solution of the two-potential equation with the polynomial testing and pulse weighting functions. Details can be found in [31].

We have assumed wires to be perfectly conducting. On the wire surface, the tangential component of the electric field must vanish, according to the first equation in (6). We separate the electric field into two components,  $\mathbf{E} = \mathbf{E}_w + \mathbf{E}_i$ . The first component ( $\mathbf{E}_w$ ) is produced by the currents and charges of the wire structure. This component is related to the potentials and field sources (currents and charges), following the principles explained in connection with equations (18) and (25). The second component ( $\mathbf{E}_i$ ) is the impressed electric field. It models the excitation of the antenna, and is assumed to be a known function. This component can be given directly or evaluated as a field produced by known impressed currents,  $\mathbf{J}_i$ .

Hence, we rewrite the boundary condition for the electric field as

$$(\mathbf{E}_w + \mathbf{E}_i)_{\text{tan}} = 0. \quad (46)$$

A transmitting antenna is driven by a lumped generator, whose dimensions are always assumed much smaller than the wavelength at the operating frequency. The input impedance (or admittance) can be defined only if we have two closely spaced terminals. If the separation between the terminals is a significant fraction of the wavelength, then there is no way to uniquely define the input parameter.

For a lumped generator, the impressed electric field is localized in a small region of a wire segment, referred to as the excitation region. Treatment of excitation regions is a delicate problem when the size of the region is above about 1/100 of the wavelength, and details can be found elsewhere [21].

A receiving antenna is excited by an incident electromagnetic wave, which may arrive at the antenna after reflections from nearby objects, like a perfectly conducting ground plane. The impressed electric field exists at all points of the receiving antenna structure.

Implementing the thin-wire approximation described in Section 3.4, we can avoid dealing with the surface integrals in equation (24). Namely, using equation (25), the two potentials can be expressed in terms of the wire current and the per-unit-length charge density, which are filamental and located on the wire surface. Now, equation (46) should be interpreted in terms of the extended boundary conditions as postulating the axial component of the total electric field to be zero on the wire axis. In the thin-wire approximation, the current is only axially directed. Changing the notation in equation (25), assuming a vacuum everywhere, the two potentials are evaluated as

$$\mathbf{A}(\mathbf{r}) = \mu_0 \int_{L'} \mathbf{u}(s') I(s') g_w(\mathbf{r}, \mathbf{r}') ds', \quad V(\mathbf{r}) = \frac{1}{\epsilon_0} \int_{L'} \rho_l(s') g_w(\mathbf{r}, \mathbf{r}') ds', \quad (47)$$

where  $\mathbf{r}$  is the position-vector of the field point,  $I(s) = 2\pi R |\mathbf{J}_s(s)|$  is the wire current and  $\rho_l = 2\pi R \rho_s$  the per-unit-length charge density,  $R$  is the wire radius,  $\mathbf{J}_s(s)$  the surface-current density,  $\rho_s$  the surface-charge density,  $s$  the local coordinate along the wire axis ( $L'$ ),  $\mathbf{u}(s')$  the unit vector of the axis,

$$g_w(\mathbf{r}, \mathbf{r}') = \frac{\exp(-jk\sqrt{|\mathbf{r} - \mathbf{r}'|^2 + R^2})}{4\pi\sqrt{|\mathbf{r} - \mathbf{r}'|^2 + R^2}} \quad (48)$$

is known as the thin-wire (reduced) kernel, and  $\mathbf{r}'$  is the position-vector of the element  $ds'$  of the wire axis.

Equations (47) and (48) produce exact results for points on the axis of a cylindrical wire segment. Otherwise, they yield a good approximation except in the immediate vicinity of discontinuities (junctions and ends).

The wire current and charge are related by the continuity equation (27). Hence, the electric field can be expressed only in terms of the wire current and its first derivative as

$$\mathbf{E}_w(\mathbf{r}) = -j\omega\mu_0 \int_s \left( \mathbf{u}(s') I(s') g_w(\mathbf{r}, \mathbf{r}') + \frac{1}{k^2} \frac{dI(s')}{ds'} \text{grad } g_w(\mathbf{r}, \mathbf{r}') \right) ds', \quad (49)$$

where the gradient is evaluated by differentiating the kernel with respect to  $\mathbf{r}$ .

The wire structure is divided into  $N$  straight segments. Each segment has its local axis ( $s_m, m=1, \dots, N$ ), which starts at one segment end, where we assume  $s_m = 0$ , and is directed towards the other segment end, where  $s_m = h_m$ , and  $h_m$  is the segment length. The reference direction for the current coincides with the orientation of the  $s$  axis. After substituting equation (49) into the boundary condition (46), the two-potential equation (also referred to as the vector-scalar-potential equation) is finally obtained as

$$\sum_{m=1}^N \int_0^{h_m} \mathbf{u}_p \cdot \left( \mathbf{u}_m I_m(s'_m) g_w(\mathbf{r}, \mathbf{r}') + \frac{1}{k^2} \frac{dI_m(s'_m)}{ds'_m} \text{grad } g_w(\mathbf{r}, \mathbf{r}') \right) ds'_m = \frac{\mathbf{u}_p \cdot \mathbf{E}_i(\mathbf{r})}{j\omega\mu_0}, \quad p = 1, \dots, N, \quad (50)$$

where  $p$  is the index of the wire segment where the boundary condition is imposed.

We omit further details here. We only note that equation (50) can be enhanced to incorporate skin-effect losses and distributed loadings by modifying the boundary condition (46), and include lumped loadings by controlled-generator models [31]. Various loadings are deliberately inserted into antennas [21]. For example, resistors are used to dampen resonances and thus increase the operating bandwidth, inductors can apparently lengthen the antenna or provide an increased gain, both at the expense of reducing bandwidth, and capacitors can improve broadband properties. Also, often the matching and filtering circuit of an antenna is analyzed simultaneously with the antenna, which extends applications of the loadings.

The presence of a perfectly conducting ground plane is replaced by the taking the image of the wire structure. Other kinds of symmetries that exist in an antenna structure may also be incorporated to expedite the analysis.

We solve equation (50) using the polynomials for expansion and pulses for testing. In [31] it is shown that the polynomial expansion is superior both in accuracy and speed compared with the pulse expansion. The current distribution,  $I_m(s_m)$ , is approximated along each wire segment by a polynomial (power series) with unknown coefficients, which amounts to an almost-entire domain approximation,

$$I_m(s_m) = \sum_{i=0}^{n_m} I_{mi} \left( \frac{s_m}{h_m} \right)^i, \quad 0 \leq s_m \leq h_m, \quad m = 1, \dots, N, \quad (51)$$

where  $n_m$  is a chosen degree of the polynomial,  $I_{mi}$  are unknown complex coefficients, and  $s_m/h_m$  is the normalized local coordinate along the segment. The total number of the unknown coefficients for a segment is  $(n_m + 1)$ . Numerical experiments have indicated that  $n_m = 4..8$  per wavelength is sufficient to yield accurate results for the antenna characteristics in most practical cases.

Expansion (51) is substituted into equation (50). A set of pulses is selected for testing. Pulses are distributed along wire segments, but there are also pulses that partly lie on pairs of wire segments at junctions. Details of the scheme can be found in [31]. An integration over a pulse located on wire segment  $p$  ( $s_{p1} < s_p < s_{p2}$ ) annihilates the gradient in (50), reducing this equation to

$$\begin{aligned} & \sum_{m=1}^N \sum_{i=0}^{n_m} I_{mi} \left( \int_{s_{p1}}^{s_{p2}} \int_0^{h_m} \mathbf{u}_p \cdot \mathbf{u}_m \left( \frac{s_m}{h_m} \right)^i g_w(\mathbf{r}, \mathbf{r}') ds'_m ds_p \right. \\ & \left. + \frac{1}{k^2} \frac{i}{h_m} \int_0^{h_m} \left( \frac{s_m}{h_m} \right)^{i-1} \left( g_w(\mathbf{r}, \mathbf{r}')_{s_{p2}} - g_w(\mathbf{r}, \mathbf{r}')_{s_{p1}} \right) ds'_m \right) \\ & = \int_{s_{p1}}^{s_{p2}} \frac{\mathbf{u}_p \cdot \mathbf{E}_i(\mathbf{r})}{j\omega\mu_0} ds_p, \quad p = 1, \dots, N. \end{aligned} \quad (52)$$

Equations of the form (52) are augmented with equations expressing Kirchhoff's current law for each junction and free wire end.

The integrals appearing in equation (52) are solved numerically. Generally, the numerical integration is the only possibility, as there is no analytical solution in most cases. The integrals that appear in antenna problems are often hard for evaluation, as the integrands have singularities or pseudosingularities when  $\mathbf{r}$  and  $\mathbf{r}'$  become close or coincide. The singularity is such that, for example, the Green's function (kernel) in equation (25) goes to infinity when  $\mathbf{r} = \mathbf{r}'$ . The kernel (48) in equation (52) is finite, but it has a very sharp peak, whose amplitude is of the order of  $1/R$ , centered at  $\mathbf{r} = \mathbf{r}'$ . This peak is referred to as the pseudosingularity.

A useful strategy is to subtract the static term, which dominates near the pseudosingularity, from the kernel (48), or even extract several terms that can be integrated analytically. The remainder is a reasonably well-behaved function, small in magnitude, so it can be integrated numerically with a satisfactory accuracy.

The resulting system of linear equations is solved for the coefficients  $I_{mi}$ , using Gaussian elimination or LU decomposition, thus yielding the approximate current distribution.

#### 4.2.4. Evaluation of antenna characteristics

Once the current distribution is known, one can relatively easily evaluate various antenna characteristics. The current distribution along the wires is readily available, as the solution has determined the expansion polynomials in equation (51). If the electric field in the antenna vicinity is required, which is referred to as the near field, it can be evaluated from (49). This field is needed, for example, to establish the safety region for humans in the vicinity of transmitting antennas (e.g., radio and TV broadcast antennas, or mobile phones), analyze corona problems associated with high-power antennas, and in EMC/EMI considerations.

However, for most practical cases, the key characteristics of an antenna are its input impedance, or, equivalently, reflection coefficient with respect to the given characteristic impedance of the feeder, and the radiation pattern. Due to reciprocity [3,4], these characteristics are identical when the antenna is in the transmitting mode as when the same antenna is in the receiving mode, although the current distributions in the two cases are different. The numerical analysis is somewhat simpler for the transmitting mode, and we consider this mode in what follows.

We consider an antenna that has only one port. We assume the antenna driven by one lumped ideal voltage generator. The driving voltage, i.e., the generator electromotive force,  $V$ , equals the integral of the impressed field ( $\mathbf{E}_i$ ) in the excitation region, along the wire axis. It is, hence, a known quantity. The numerical analysis yields the current distribution and, consequently, the current at the generator ( $I_0$ ). The antenna input admittance is simply  $Y = I_0/V$ . It is now a straightforward matter to evaluate the input impedance and the reflection coefficient with respect to a given reference impedance.

A multiport antenna is characterized by an admittance, impedance, or scattering matrix. The simplest procedure is to evaluate the admittance matrix,  $[\mathbf{y}]$ , first, by driving the antenna one port at a time, following a similar procedure as for a single-port antenna. The other two matrices can be evaluated by matrix manipulations as explained in [31]. If the multiport antenna is actually an antenna array, then one of these three matrices could be needed to solve for the feeding voltages by analyzing the feeding network terminated with the antenna matrix.

Thereafter, the array is analyzed with all ports simultaneously driven by these voltages to evaluate the radiation pattern.

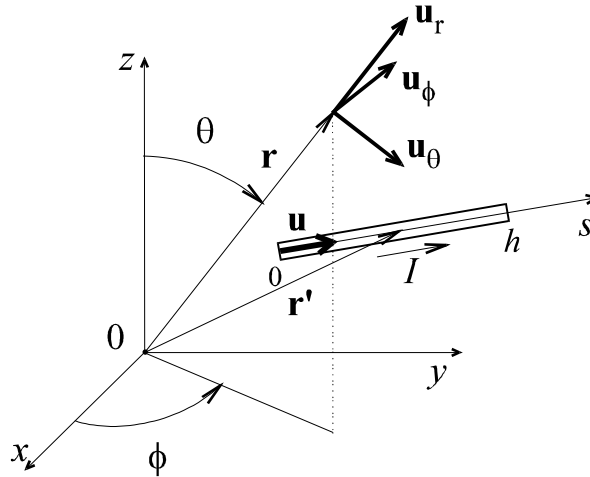


Figure 8. Coordinate system for evaluation of far fields.

The far (radiated) electric field of an antenna is related to the magnetic vector-potential as (Figure 8)

$$\mathbf{E} = j\omega \mathbf{u}_r \times (\mathbf{u}_r \times \mathbf{A}), \quad (53)$$

where  $\mathbf{u}_r$  is the unit vector directed from the coordinate origin (located in the antenna vicinity) towards the field point. We suppress indices "w" and "i" with the vector  $\mathbf{E}$ , as in the far-field zone of a transmitting antenna the impressed currents usually radiate negligibly and the impressed electric field does not exist. Hence, only the antenna currents and charges produce the radiated fields. The radiated electric field has only the transverse components with respect to the radius-vector ( $\mathbf{r}$ ). In spherical coordinates,

$$\mathbf{E} = E_\theta \mathbf{u}_\theta + E_\phi \mathbf{u}_\phi, \quad (54)$$

where  $\mathbf{u}_\theta$  and  $\mathbf{u}_\phi$  are the unit vectors of the spherical coordinate system. In the far-field zone, at a point with spherical coordinates  $(r, \theta, \phi)$ , instead of using the first of equations (47), the magnetic vector-potential can be evaluated in a simpler way by neglecting variations of  $|\mathbf{r} - \mathbf{r}'|$  in the denominator of Green's function, leading to the following expression for the radiated electric field:

$$\mathbf{E}(\mathbf{r}) = -j\omega \frac{\mu_0}{4\pi} \frac{\exp(-jkr)}{r} \int_0^h \left( \mathbf{u}_\theta (\mathbf{u}_\theta \cdot \mathbf{u}(s')) + \mathbf{u}_\phi (\mathbf{u}_\phi \cdot \mathbf{u}(s')) \right) I(s') \exp(jk\mathbf{r}' \cdot \mathbf{u}_r) ds', \quad (55)$$

where  $r = |\mathbf{r}|$ . The radiated magnetic field is related to the electric field by

$$\mathbf{H} = \frac{\mathbf{u}_r \times \mathbf{E}}{\zeta_0}, \quad (56)$$

where  $\zeta_0 = \sqrt{\mu_0 / \varepsilon_0}$  is the wave impedance (intrinsic impedance) of a vacuum.

The Poynting vector can be evaluated from (20) or (21), as appropriate. The power gain (with respect to an isotropic radiator) is then given by

$$G_p = \frac{|\mathbf{P}|}{P_{\text{fed}}} 4\pi r^2, \quad (57)$$

where  $P_{\text{fed}}$  is the average power fed to the antenna, which can be evaluated from the voltages and currents at the antenna ports. The power fed to the antenna in the transmitting mode is  $P_{\text{fed}} = P_{\text{rad}} + P_{\text{loss}}$ , where  $P_{\text{rad}}$  is the radiated power and  $P_{\text{loss}}$  is the loss power. The antenna efficiency is  $\eta = P_{\text{rad}} / P_{\text{fed}}$ , and the directive gain is  $G_d = G_p / \eta$ . In decibels, the gain (power or directive) is evaluated as  $g = 10 \log_{10} G$  dBi.

#### 4.2.5. Examples

Two examples of the analysis of wire antennas follow to illustrate the capabilities of the MoM solution.

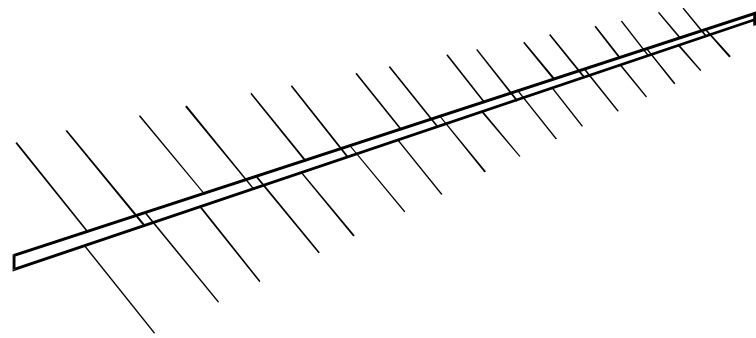
The first example is a log-periodic dipole array for UHF TV reception, with 16 elements, shown in Figure 9a. The antenna has a feeding line made of two booms (rods) of a square cross section, which form a two-wire line. The dipoles are attached to this line, with alternating orientations to provide the required phasing of the dipole excitations. The dipoles are made of wires that have a circular cross section. The input port to the antenna is at the "nose", where a  $75\ \Omega$  coaxial cable is attached. The cable passes through one of the booms, but the cable is not included in the computer simulation. In the wire-antenna model the booms were replaced by equivalent conductors of a circular cross section. The equivalence is such as to keep intact the characteristic impedance of the feeder. The dipoles and the feeder were then analyzed using program [31], as a unique wire structure.

Figure 9b shows the input reflection coefficient of the antenna, computed and measured on a laboratory prototype. In measurements, there were two major difficulties that affected the quality of the results. First, the network analyzer was a  $50\ \Omega$  system, so minimum-loss pads were inserted to convert it to a  $75\ \Omega$  system. The second problem was the calibration. A commercial  $75\ \Omega$  coaxial cable (1 m long) was used to check the antenna performance under realistic practical conditions. The cable was attached to the antenna two-wire feeder by pigtailed, and by a connector on the other side. A precise calibration of the network analyzer was performed at the reference plane of this connector, as the calibration kit could not be connected to the pigtailed.

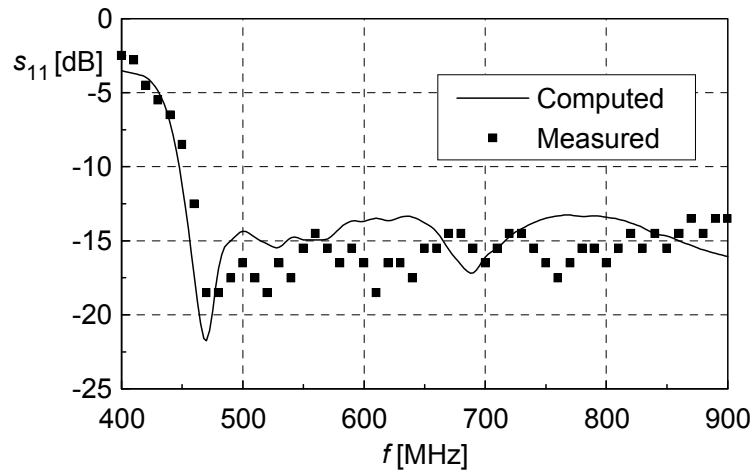
Figure 9c shows the radiation pattern of the antenna, measured in outdoor conditions. Some small reflections can be noted in the measured pattern, causing an asymmetry. In spite of all these problems, the agreement between the theory and experiment can be qualified as satisfactory for most practical purposes.

The second example is a GPS ring-resonator antenna, designed for the L2 band, shown in Figure 10a [35]. The antenna consists of a ring, placed parallel to a ground plane, and two capacitive probes. The ring and the plane play the role of a re-entrant resonator. The objective is to excite a traveling wave on the ring, of a proper orientation. The ring current corresponding to this wave will then radiate a circularly polarized wave in the zenith direction. The ring resonator is excited by one vertical probe (a piece of wire), fed by a coaxial line of a  $50\ \Omega$  characteristic impedance. The probe is capacitively coupled to the ring. However, was this probe alone, it would excite two waves traveling in opposite senses, which would correspond to a standing wave. The antenna would then radiate a linearly polarized wave. One of the two traveling waves can be suppressed by using another, grounded probe, which is capacitively coupled to the ring at an optimal location. The ring is supported by two plastic poles, which add small parasitic capacitances between the ring and the ground.

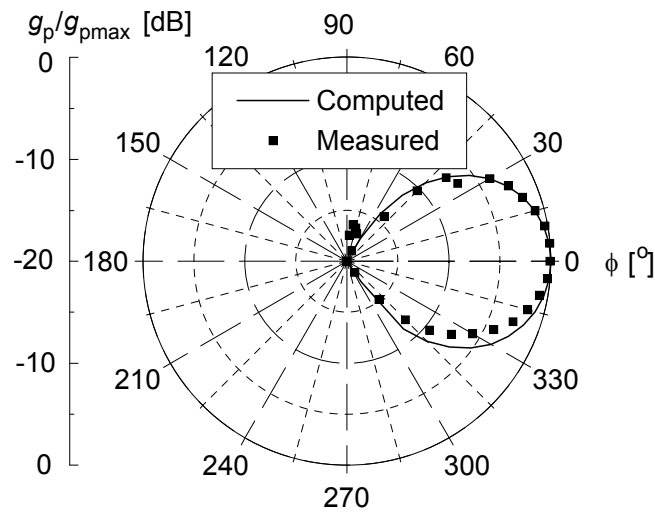
Figure 10b shows the computed and measured reflection coefficient of the antenna, demonstrating a good agreement. Figure 10c shows the computed antenna power gain in the zenith direction and the axial ratio of the polarization ellipse. The axial ratio is the ratio of the major to the minor axis of the ellipse. If the axial ratio is 1 (i.e., 0 dB), a perfect circular polarization is obtained. For GPS applications, an RHC (right-hand circular) polarization is required, which is provided by the disposition of the feeding and passive capacitive probes as in Figure 10a. Reversing the roles of the probes would yield an LHC (left-hand circular) polarization.



(a)



(b)



(c)

Figure 9. A 16-element log-periodic dipole array: (a) sketch, (b) input reflection coefficient with respect to  $75 \Omega$  ( $s_{11}$ ) as a function of frequency ( $f$ ), and (c)  $E$ -plane radiation pattern at 760 MHz: relative power gain ( $g_p / g_{pmax}$ ) as a function of azimuth angle ( $\phi$ ).

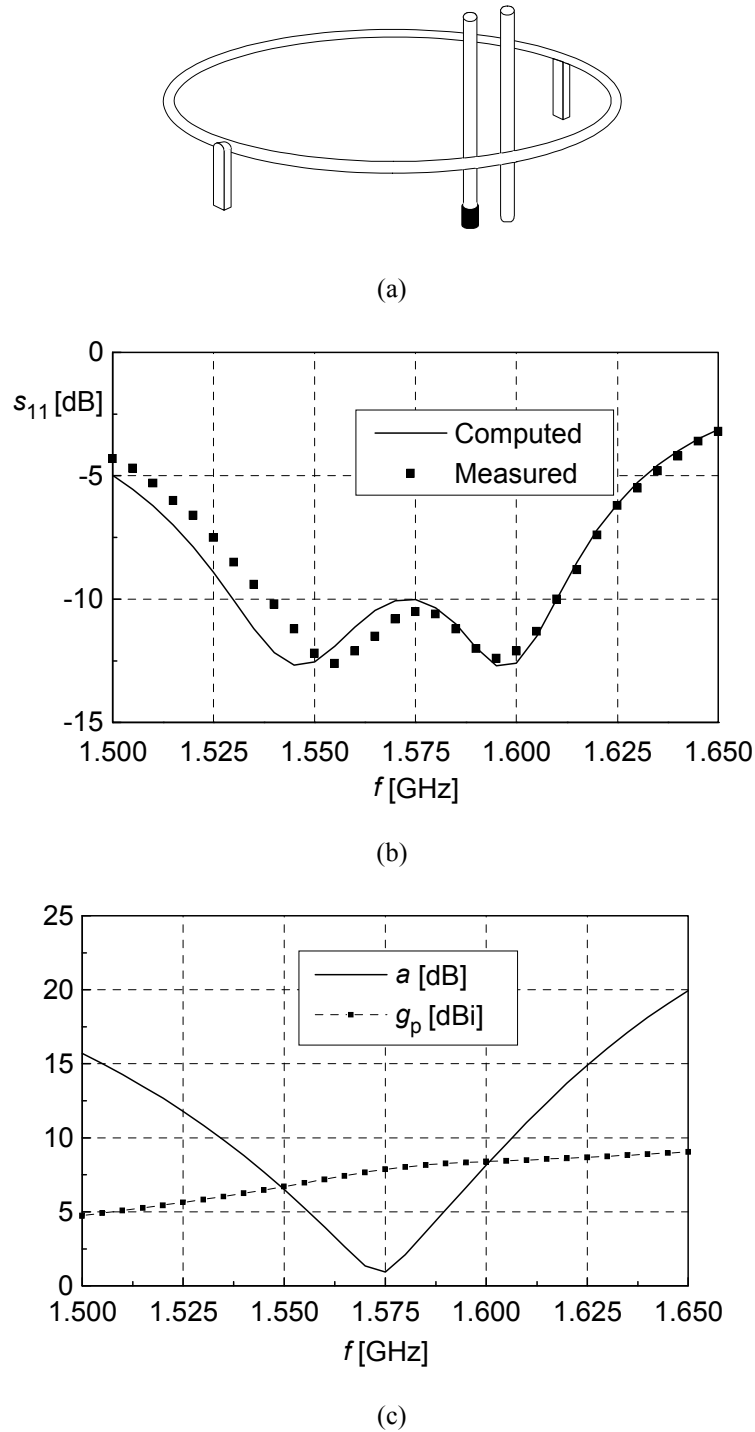


Figure 10. A ring antenna for right-hand circular polarization: (a) sketch, (b) input reflection coefficient with respect to  $50 \Omega$  ( $s_{11}$ ) as a function of frequency ( $f$ ), and (c) axial ratio ( $a$ ) and power gain ( $g_p$ ) in zenith direction as a function of frequency ( $f$ ).

### 4.3. Metallic (surface) antennas

#### 4.3.1. Definition of metallic antennas

In this section we analyze perfectly conducting (PEC) bodies and surfaces. They are assumed placed in a vacuum. This is an approximation of real metallic bodies and surfaces that always have some losses.

The currents and charges on a PEC body (Figure 11a), due to the skin-effect, are localized on the surface of the body ( $S$ ). This surface is, of course, closed. Since there are no electromagnetic fields in the interior region of the body, i.e., within the space enclosed by  $S$ , we can assume this region filled by a vacuum instead by the PEC. Hence, we can reduce the body to an empty, zero-thickness shell (Figure 11b), i.e., a closed PEC surface ( $S$ ), without affecting the fields in the exterior space. The analysis of closed PEC surfaces, in turn, can follow the same steps as the analysis of open PEC surfaces. This is the reason why we treat PEC bodies and surfaces in a unique way.

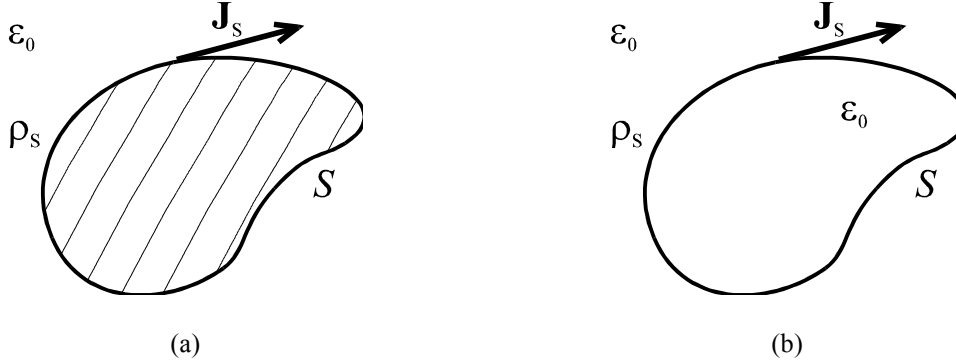


Figure 11. A PEC body (a) can be replaced by a zero-thickness PEC shell (b).

Basically, radiation and scattering by PEC surfaces is analyzed following similar guidelines as the analysis of PEC wire structures. One starts from an appropriate boundary condition, expresses fields in terms of sources using potentials, and formulates an integral equation for the current distribution. This equation is then solved following the general MoM steps. However, the analysis of surfaces is a more complex problem than the analysis of wire structures. There are three major reasons.

The first one is that no approximation similar to the thin-wire approximation can be made for arbitrary surfaces. Hence, the potentials in equation (18) must be evaluated in terms of the field sources (surface currents and charges) using surface integrals as in equation (24), except that  $\epsilon$  and  $\mu$  should be substituted by  $\epsilon_0$  and  $\mu_0$ , respectively. Integration in (24) is a much more complicated task than the evaluation of single integrals in (47). An exception is PEC bodies of revolution [36], for which the starting equation for the analysis can be fully reduced to the thin-wire integral equation, (50).

The second reason is the dimensionality of the unknowns. For wires the unknown current distribution is a function of only one coordinate, i.e., the local coordinate along the wire axis. For surfaces the current distribution is a function of two coordinates, e.g., two local coordinates of a system bound to the surface. Hence, the basis functions must be more complicated. This means two things. First, if a segmentation of the surface is used, which is needed both for subdomain and almost-entire-domain approximations, it must be two-dimensional. For example, the surface is divided into a set of triangles [37] or quadrilaterals [38,32]. Second, the basis function defined on a subdomain is most often such that it depends on two coordinates. (If it is taken to depend only on one local coordinate, it amounts to a piecewise-constant approximation in terms of the other coordinate.) As a result, the number of unknowns required to analyze a "simple" surface, such as a rectangular plate, is approximately proportional to the frequency squared. Alternatively speaking, it is proportional to the surface area divided by the wavelength squared. The number of unknowns for a "simple" wire is linearly proportional to the frequency, which is substantially less than for a rectangular plate of similar linear dimensions.

The third reason is that the surface-current density is a vector quantity that has two components. In a numerical solution, we need to approximate both components, which further doubles the number of unknowns.

### 4.3.2. Integral equations and their solution

We have seen that electrostatic problems and wire antennas are analyzed starting from the boundary condition for the electric field, or, equivalently, for the scalar-potential in electrostatics. An analog approach can be applied to the analysis of perfectly conducting surfaces, resulting in an EFIE. This equation has a form analogous to that for wire antennas, except for having surface integrals, and the currents and charges being functions of two local coordinates in the surface. The EFIE for PEC surfaces thus reads

$$\int_{S'} \mathbf{u}(\mathbf{r}) \cdot \left( \mathbf{J}_s(\mathbf{r}') g(\mathbf{r}, \mathbf{r}') + \frac{1}{k^2} \text{div}'_s \mathbf{J}_s(\mathbf{r}') \text{grad} g(\mathbf{r}, \mathbf{r}') \right) dS' = \frac{\mathbf{u}(\mathbf{r}) \cdot \mathbf{E}_i(\mathbf{r})}{j\omega\mu_0}, \quad (58)$$

where  $S'$  coincides with the surface  $S$  of the PEC body, Green's function  $g(\mathbf{r}, \mathbf{r}')$  is given by (23),  $\text{div}'$  denotes differentiation with respect to  $\mathbf{r}'$ , and  $\mathbf{u}(\mathbf{r})$  is the unit vector tangential to  $S$  at the point defined by  $\mathbf{r}$ . The

differentiation implied by the  $\text{grad}$  operator is performed with respect to  $\mathbf{r}$ . There are, generally, two local components of the vector  $\mathbf{J}_s$ . Consequently, to provide a sufficient number of conditions, two orthogonal vectors  $\mathbf{u}(\mathbf{r})$  are used at any point in (58); resulting in a pair of scalar equations for any  $\mathbf{r}$ . Equation (58) can be applied to both open and closed PEC surfaces.

Based on the boundary condition for the magnetic field, i.e., the second equation in (6), one can formulate an MFIE for closed PEC surfaces. For open surfaces, an MFIE can not be set due to difficulties encountered with distinguishing between the fields and surface currents on the two faces of the zero-thickness surface. Hence, the EFIE is usually the preferred choice.

For closed PEC surfaces, there exists, however, a problem of spurious solutions associated with both the EFIE and MFIE. The spatial region encompassed by the surface is an ideal electromagnetic resonator, which, theoretically, can support free oscillations at a set of discrete resonant frequencies. The resonant field is confined to this region and it is not coupled with the surrounding space. Hence, such a field can not be induced by an external field. However, a solution of the EFIE (or MFIE) can not distinguish between currents induced on the inner and outer faces of the PEC shell. Due to various approximations and errors involved in the numerical procedure, in the vicinity of resonant frequencies the solution for the current distribution contains spurious components, which are similar to the theoretical resonant modes. These spurious components create a non-zero field in the spatial region outside  $S$  because they are not identical to the resonant modes. Hence, they modify the field in the exterior of the PEC surface and cause errors in the numerical results for the input impedance and radiation pattern of the analyzed antenna.

The problem of spurious solutions can be bypassed in several ways, which include an artificial insertion of losses in the system [39] and modifications of the integral equation, like a combination of the EFIE and the MFIE [40,41].

Among a variety of useful and efficient approximations for the current distribution on PEC bodies, we stress two techniques. The first one [37] is a subdomain approximation. The surface of the PEC body is divided into a set of triangular patches. A basis function is defined on a pair of adjacent triangles for one component of the surface-current density vector ( $\mathbf{J}_{sp}$ ), as shown in Figure 12a. The basis function is such that there is no current flow outside these two triangles. On the common edge of the two triangles, the normal components of  $\mathbf{J}_{sp}$  are equal on both triangles. Hence, the continuity equation is automatically satisfied for the triangle edges without creating line charges on the edges. The direction of the vector  $\mathbf{J}_{sp}$  on a triangle is radial with respect to the vertex, i.e., it has the direction of the corresponding radius-vector  $\boldsymbol{\rho}$  in Figure 12a. The intensity of the vector  $\mathbf{J}_{sp}$  is a linear function of  $|\boldsymbol{\rho}|$ . On each triangle, except for triangles that are at the boundary of the surface, there are three such basis functions defined, each of them tangential to the triangle surface. When added, these three vectors yield the resulting current density vector. This approximation of the current density over a triangle results in a constant charge density on that triangle, which amounts to a pulse approximation for the surface charges.

The second technique [38,32] divides the surface into a set of so-called bilinear surfaces (quadrilateral patches). On each patch, shown in Figure 12b, the current density is split into two components ( $\mathbf{J}_{ss}$  and  $\mathbf{J}_{sp}$ ) with respect to a local  $ps$  coordinate system. Each component is approximated by a power series (polynomial). The polynomials are constructed such that the continuity is satisfied for the normal component of the current over each edge, as for the triangular patches. Individual quadrilateral patches can be relatively large, of the order of a wavelength in linear dimensions, which helps reduce the number of unknowns at the expense of much harder basic integrals that are to be evaluated numerically. The charge density associated with the approximate current distribution is also a polynomial function, and it is thus smooth over a patch. This results in a better-behaved local field than for the pulse approximation, which further adds to the accuracy of the method.

Regardless of the set of expansion functions used, we approximate a given surface by a set of relatively simple, special surfaces, like triangles and quadrilaterals for the above quoted techniques. Hence, we not only approximate the variations of the vector  $\mathbf{J}_s$ , but also approximate the original surface  $S$  by a composite surface consisting of a number of smaller (subdomain) surfaces, as depicted in Figure 4. This approximation of the geometry should be performed with care, to minimize the associated error. For example, if we approximate a sphere by a set of triangles, the original sphere should be between the inscribed and circumscribed sphere with respect to the triangularized surface. In particular, we may postulate the original sphere and the triangularized surface to have the same surface area or to encompass the same volume.

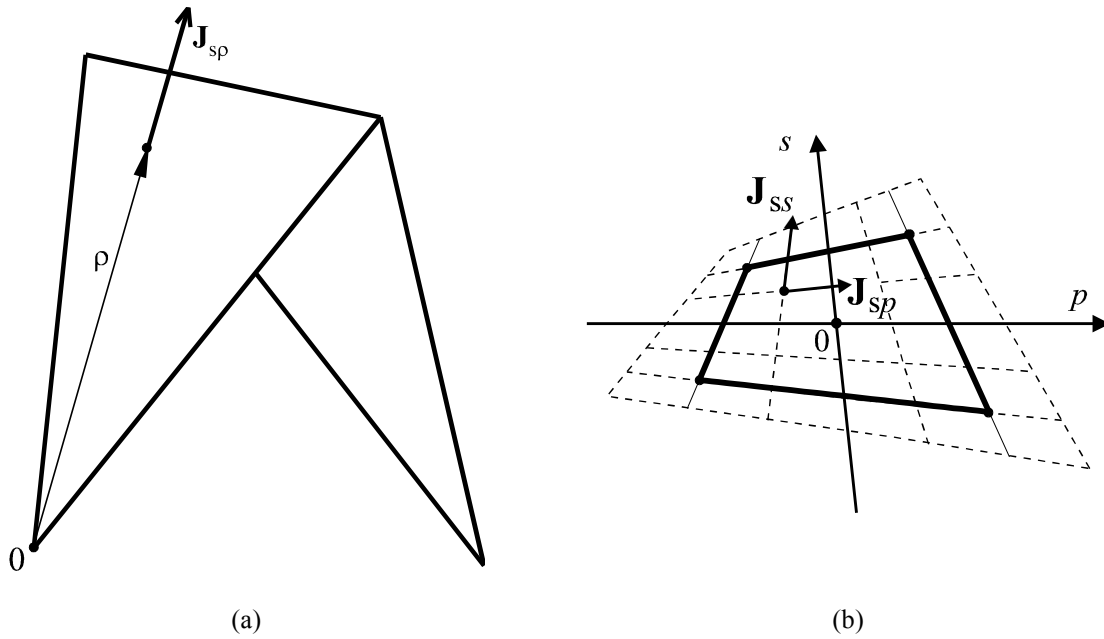


Figure 12. Two basis functions for the analysis of surface antennas: (a) triangular patches, and (b) quadrilateral patches.

Losses in real conductors can be accounted for by the perturbation technique [2] if the skin-effect is fully pronounced. Instead of having a zero tangential component of the electric field, as postulated by the first equation in (6), we have a modified boundary condition that this field component is proportional to the density of the surface currents, where the proportionality coefficient is the intrinsic (wave) impedance of the metal,  $Z_m$ . So, instead of the first condition in (6), we have

$$\mathbf{n} \times \mathbf{E}_1 = Z_m \mathbf{n} \times \mathbf{J}_s . \tag{59}$$

The intrinsic impedance is given by  $Z_m = \sqrt{\frac{j\omega\mu}{\sigma}}$ , where  $\mu$  is the permeability and  $\sigma$  the conductivity of the metal.

This impedance is complex, and its real part is referred to as the surface resistance. The modified boundary condition does not impose a particular complication in the numerical solution, but one should take care about the conditions under which equation (59) is valid.

A special problem is the combined analysis of wires and PEC surfaces. If one wants to preserve the simplicity of the analysis of wires, but to include surfaces as well, there is a need to carefully model attachments (junctions) of wires to PEC surfaces. One technique is to define attachment modes [42]. Such a mode is a special current distribution that exists on the metallic surface in the vicinity of the junction. This distribution continues into the wire current at the center of the junction area, and it vanishes at a certain distance from the junction. Another technique is to subdivide the metallic plate (Figure 13) so that the surface current on the plate is concentrated in the junction area and has a continuous transition to the wire current without introducing any special current distribution [43].

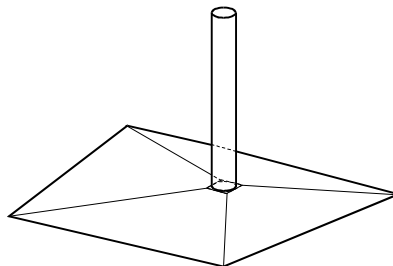


Figure 13. Modeling of attachment of a wire to a metallic plate, by subdividing the plate into four quadrilaterals.

Once the current distribution on the surfaces and wires is known, antenna characteristics can be evaluated following similar guidelines as described in Section 4.2.4.

### 4.3.3. Examples

As the first example of analysis of metallic antennas we consider the UHF TV panel antenna shown in Figure 14a [44]. The antenna consists of two flat dipoles, placed parallel to a finite-size conducting reflector. The dipoles are supported by posts. The dipoles are fed by a coaxial line that passes through one of the posts, and continues into the horizontal two-wire lines. The supporting posts act like a balun. The antenna was analyzed numerically using the program of reference [32]. Figure 14b shows the computed and measured antenna input impedance. An excellent agreement between the two sets of data can be observed.

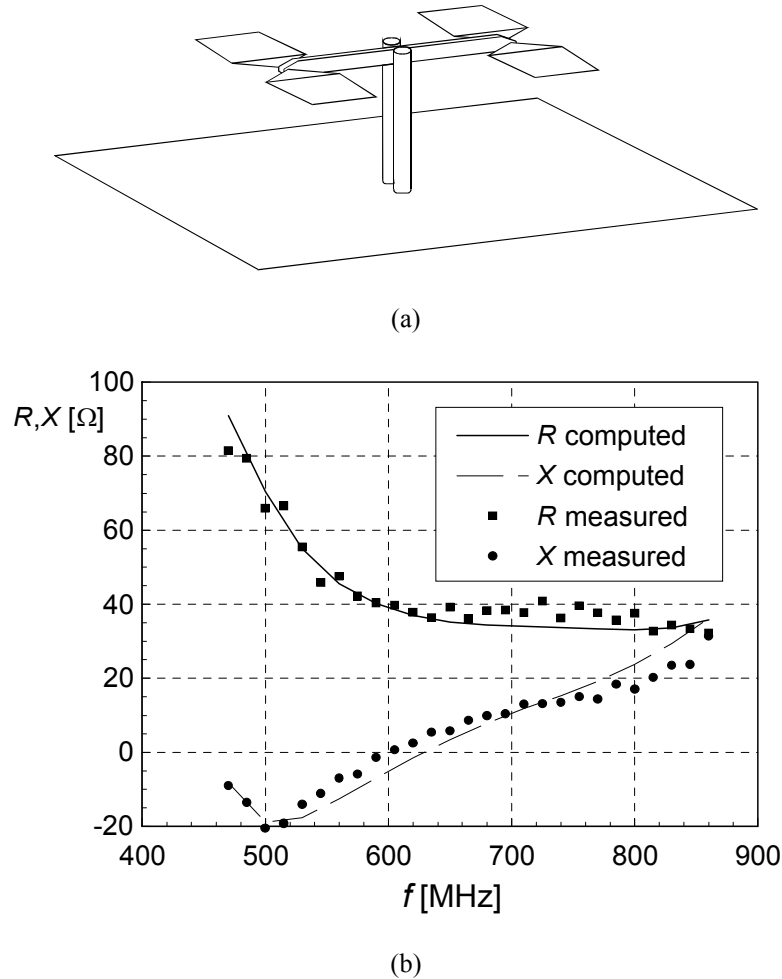


Figure 14. A panel UHF TV antenna: (a) sketch and (b) input resistance ( $R$ ) and reactance ( $X$ ) as a function of frequency ( $f$ ).

As the second example we consider the rectangular horn antenna shown in Figure 15a. The horn is fed by a rectangular waveguide, and the waveguide is excited by a small dipole placed inside. Figure 15b shows results for the radiation pattern of the antenna, computed using the program of reference [32] along with experimental results from reference [45], again demonstrating an excellent agreement.

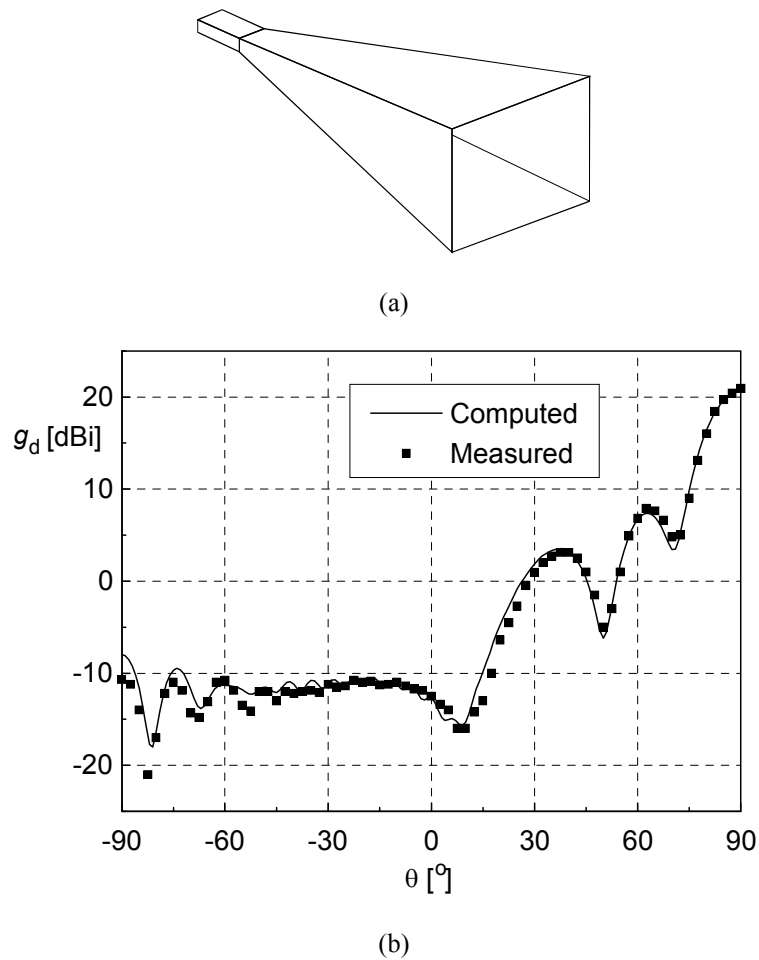


Figure 15. A rectangular horn antenna: (a) sketch and (b)  $E$ -plane radiation pattern: directive gain ( $g_d$ ) as a function of zenith angle ( $\theta$ ).

## 4.4. Metallo-dielectric antennas

### 4.4.1. Definition of metallo-dielectric antennas

Most practical antennas are made of various materials, which include good conductors (metallic parts) and dielectrics (insulators). In some cases, the dielectric parts do not play a vital role in the antenna electrical performance. For example, these parts can serve only as a mechanical support, like insulators in guy ropes of LF and MF tower antennas, or they can cover the antenna to protect it, like a radome. In other cases, the dielectrics are deliberately placed to modify some properties of the antenna. For example, a high-permittivity dielectric substrate is used to reduce the size of a printed-circuit (patch) antenna. Materials can also have magnetic properties, but this is beyond our scope here. To add to the complexity, the conductors are never perfect and dielectrics also have certain losses. Even superconductors have a finite surface resistance at high frequencies, which increases as frequency squared. Electromagnetic analysis of structures that consist of a variety of materials is one of the hardest numerical problems.

In contrast to the situation described in Sections 4.2 and 4.3, where PEC wires and surfaces were embedded in a homogeneous medium (a vacuum), we deal here with an inhomogeneous medium. Generally, the medium properties, characterized by the permittivity, conductivity, and permeability, are arbitrary functions of the spatial position. In many practical cases, however, the medium is homogeneous within certain regions, and material properties change abruptly at their boundary surfaces. For example, for an ordinary printed-circuit antenna, one region with a homogeneous dielectric is the substrate, and the surrounding medium is a vacuum, which is another homogeneous region. Such cases are referred to as piecewise-homogeneous media.

There exist several basic approaches to the analysis of electromagnetic systems that consist of a variety of materials. We shall divide them into three groups. The first two groups are based on integral equations. One of them is founded on the volume equivalence theorem and results in a volume integral equation. The other stems from the surface equivalence theorem and results in surface integral equations. The third group is based on differential

equations, and it includes the finite-element method (FEM) and the finite-difference method (FD). In this chapter, we briefly describe only the FEM, whereas another chapter of this book is devoted to the FD approach.

#### 4.4.2. Volume integral equation and its solution

For antennas that consist of conductors and dielectrics the field sources are electric currents and charges induced in conductors, as well as polarization charges and polarization currents throughout dielectric volumes. The conductor currents and charges are pure surface sources for a perfect conductor, but they are distributed throughout the conductor volume in the case of an imperfect, real conductor. In a leaky dielectric, there also exist volume conduction currents and associated free charges. However, mathematically, they can automatically be taken into account through the imaginary part of the dielectric complex permittivity. All these sources produce the electromagnetic fields as if they were located in a vacuum. This is because these sources completely replace the conducting and dielectric bodies with respect to the electric field ( $\mathbf{E}$ ) and the magnetic flux-density ( $\mathbf{B}$ ) they create. This fact is basically the statement of the volume equivalence theorem [3,4].

The approach to analyzing antennas that consist of conductors and dielectrics is to explicitly find all the field sources, by solving an appropriate integral equation [46-50].

For simplicity, we first consider scattering from the dielectric body shown in Figure 16a. The body is located in a vacuum. We assume to know the impressed (illuminating) electric field ( $\mathbf{E}_i$ ), e.g., the electric field of an incident plane wave. As the consequence of the illumination, polarization currents and charges are induced in the body, which create electromagnetic fields at any point within the body and outside the body. We also assume the permittivity ( $\epsilon$ ) of the material to be a differentiable function of spatial coordinates, whereas the permeability is  $\mu_0$  everywhere. Hence, the only surface of discontinuity is the surface  $S$  bounding the body, where the material parameters have an abrupt change. In this case the field sources are volume polarization currents ( $\mathbf{J}_p$ ) and charges ( $\rho_p$ ), which are spread within the volume bounded by the surface  $S$ , and surface polarization charges ( $\rho_{sp}$ ) spread over the surface. All these sources are assumed located in a vacuum. They can be determined starting from a properly adopted constitutive equation.

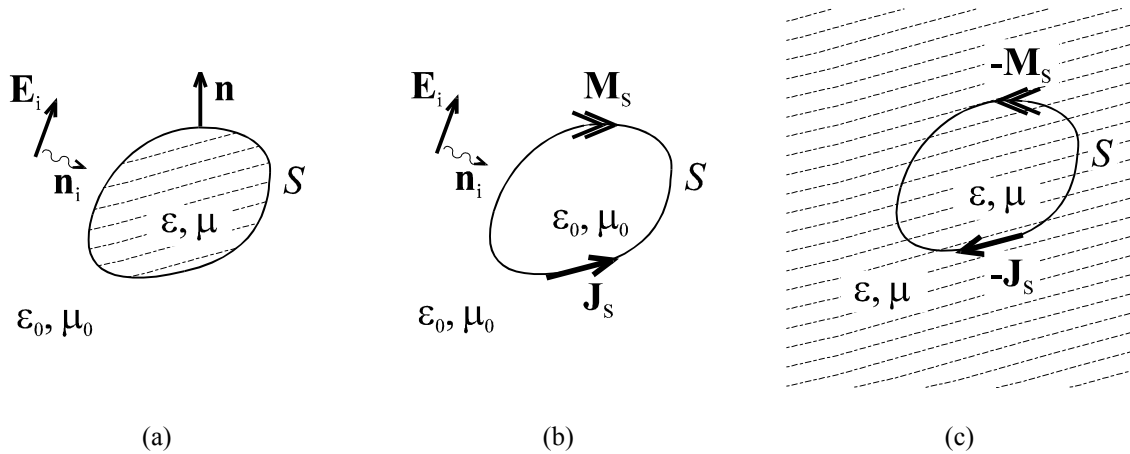


Figure 16. Illustration of the equivalence theorems: (a) a dielectric body illuminated by an incident plane wave, and equivalent systems for (b) the exterior region and (c) the interior region.

We start with the first constitutive equation in (3). It can be written in a more general form, which includes the polarization vector ( $\mathbf{P}$ ), as

$$\mathbf{D} = \epsilon_0 \mathbf{E} + \mathbf{P} . \quad (60)$$

Combining (3) and (60), the polarization vector is related to the electric field as  $\mathbf{P} = \frac{\epsilon - \epsilon_0}{\epsilon} \mathbf{E}$ . Since the density of the volume polarization currents is related to the polarization vector as  $\mathbf{J}_p = j\omega \mathbf{P}$ , the polarization currents are related to the electric field as

$$\mathbf{J}_p = j\omega \frac{\epsilon - \epsilon_0}{\epsilon} \mathbf{E} . \quad (61)$$

This equation actually represents another form of the constitutive relation for the dielectric.

Let us express the electric field vector on the right side of equation (61) in terms of the known excitation and unknown sources. First, we separate the electric field into two components,  $\mathbf{E} = \mathbf{E}_p + \mathbf{E}_i$ , where  $\mathbf{E}_p$  is the electric field produced by the polarization currents and charges, and  $\mathbf{E}_i$  is the impressed electric field. The electric field  $\mathbf{E}_p$  at an arbitrary point can now be evaluated using the first equation in (18), i.e., as  $\mathbf{E}_p = -j\omega\mathbf{A} - \text{grad } V$ , where  $\mathbf{A}$  and  $V$  are potentials produced by the polarization currents and charges placed in a vacuum. Having in mind expressions (22) and (24), these potentials can be expressed as

$$\mathbf{A}(\mathbf{r}) = \mu_0 \int_{v'} \mathbf{J}_p(\mathbf{r}') g(\mathbf{r}, \mathbf{r}') dv', \quad V(\mathbf{r}) = \frac{1}{\epsilon_0} \left( \int_{v'} \rho_p(\mathbf{r}') g(\mathbf{r}, \mathbf{r}') dv' + \int_{S'} \rho_{sp}(\mathbf{r}') g(\mathbf{r}, \mathbf{r}') dS' \right), \quad (62)$$

where  $v'$  denotes the spatial region enclosed by  $S$ , whereas the surfaces  $S'$  and  $S$  coincide. Finally, the volume polarization charges are related to the polarization currents by the continuity equation,

$$\text{div } \mathbf{J}_p = -j\omega\rho_p. \quad (63)$$

and the surface polarization charges are related to the polarization currents by the corresponding boundary condition,

$$\rho_{sp} = \mathbf{n} \cdot \mathbf{P} = \frac{\mathbf{n} \cdot \mathbf{J}_p}{j\omega}, \quad (64)$$

where  $\mathbf{n}$  is the unit outward normal on  $S$  and  $\mathbf{P}$  is the polarization vector in the dielectric at the inner face of  $S$ .

By substituting the resulting expression for the electric field into equation (61), a volume integral equation (VIE) for the volume polarization currents is obtained. In this equation the unknown vector  $\mathbf{J}_p$  appears both under the integral and as a free term.

To solve this integral equation using the MoM, we have to expand the volume polarization currents. This is a more complicated task than for the PEC surfaces in Section 4.3.2, as there are three components of the vector  $\mathbf{J}_p$ , which depend on three spatial coordinates. Several notable techniques have been published. For example, in [48] the basis functions are tetrahedrons, which are a 3D generalization of the triangular patches from [37]. In [50] the basis functions are almost-entire-domain polynomials in terms of three spatial coordinates defined in large hexahedrons.

For an antenna problem, we need to include some metallic wires and plates. If the conductors are assumed perfect, on their surfaces there exist surface currents ( $\mathbf{J}_s$ ) and charges ( $\rho_s$ ). In addition, there are surface polarization charges at the conductor surfaces, which add to the conductor charges to yield the total charges,  $\rho_{st} = \rho_s + \rho_{sp}$ . Contribution of all these sources should be included into equations (62), resulting in

$$\mathbf{A}(\mathbf{r}) = \mu_0 \left( \int_{v'} \mathbf{J}_p(\mathbf{r}') g(\mathbf{r}, \mathbf{r}') dv' + \int_{S'} \mathbf{J}_s(\mathbf{r}') g(\mathbf{r}, \mathbf{r}') dS' \right), \quad V(\mathbf{r}) = \frac{1}{\epsilon_0} \left( \int_{v'} \rho_p(\mathbf{r}') g(\mathbf{r}, \mathbf{r}') dv' + \int_{S'} \rho_{st}(\mathbf{r}') g(\mathbf{r}, \mathbf{r}') dS' \right), \quad (65)$$

where now  $S'$  denotes the union of all surfaces of discontinuity, i.e., the dielectric boundary surface and the conductor surfaces. The densities of the conductor surface currents and free charges are related by equation (26).

For the PEC surfaces the boundary condition for the tangential component of the electric field (6) still holds. Hence, for a composite structure consisting of dielectric and PEC objects a set of two integral equations is formulated. One equation is obtained by imposing the boundary condition (6) for the PEC surfaces and expressing the electric field in terms of the current distributions  $\mathbf{J}_s$  and  $\mathbf{J}_p$ . The other equation is obtained from the constitutive relation (61) in an analog way as explained above for the dielectric scatterer. In the numerical solution of these equations one has to expand the conductor currents as in Section 4.3.2, and the polarization currents as explained above.

The approach based on the volume integral equation inherently requires a large number of unknowns, as one has to approximate field sources within volumes. However, it can efficiently handle arbitrarily inhomogeneous media, unlike the approach described in the following section.

#### 4.4.3. Surface integral equations and their solution

This approach is tailored for piecewise-homogeneous media. It is based on the surface equivalence theorem [3,4]. This theorem, basically, states the following. If we consider a spatial region, encompassed by a closed surface

$S$ , all field sources outside this region can be substituted by fictitious (equivalent) surface electric and magnetic currents ( $\mathbf{J}_s$  and  $\mathbf{M}_s$ ), placed on  $S$ , without affecting the field in the region considered. The region under consideration can also be the space external to  $S$ . Such a region is assumed bounded by  $S$  and by a closed surface at infinity.

Note that magnetic currents are a mathematically introduced quantity as being dual to the electric currents. They enable a symmetrization of Maxwell's equations and boundary conditions. More details about these currents can be found, for example, in reference [3].

As an example of the application of this theorem, we consider a body made of a homogeneous dielectric (Figure 16a), of parameters  $\epsilon$  and  $\mu$ , located in a vacuum, in an incident electromagnetic field. The polarization currents and charges are induced in the body create electromagnetic fields inside and outside the body, as in the corresponding example in Section 4.4.2.

If we now consider the outer region, i.e., the region exterior to  $S$ , the fields due to the induced polarization currents and charges can be, according to the surface equivalence theorem, substituted by the fields produced by the equivalent surface currents on  $S$  (Figure 16b). The substitution means that the equivalent surface currents are placed on  $S$ , and the original field sources within  $S$  are removed. The densities of the equivalent currents are related to the electric and magnetic field ( $\mathbf{E}$ , viz.  $\mathbf{H}$ ) on the outer face of  $S$  by

$$\mathbf{J}_s = \mathbf{n} \times \mathbf{H}, \quad \mathbf{M}_s = -\mathbf{n} \times \mathbf{E}, \quad (66)$$

where  $\mathbf{n}$  is the outside normal to  $S$ . Starting from the boundary conditions and using the uniqueness theorem [3,4], it can be proven that the electromagnetic fields inside  $S$  are zero in the system of Figure 16b. If the fields within a region are zero, the material parameters of that region are irrelevant since nothing is induced in the region. Hence, we can assume the medium within the region inside  $S$  to be a vacuum, as in the outside region. Having now a homogeneous medium everywhere, we can use the standard expression for the potentials. In the presence of the magnetic currents, a total of four potentials are needed. The magnetic vector-potential and the electric scalar potential are still given by equations (24), with  $\epsilon$  and  $\mu$  replaced by  $\epsilon_0$  and  $\mu_0$ , respectively. The new potentials are the electric vector potential ( $\mathbf{F}$ ) and the magnetic scalar-potential ( $V_m$ ). In a homogeneous medium of parameters  $\epsilon$  and  $\mu$  these two potentials for surface sources are given by

$$\mathbf{F}(\mathbf{r}) = \epsilon \int_{S'} \mathbf{M}_s(\mathbf{r}') g(\mathbf{r}, \mathbf{r}') dS', \quad V_m(\mathbf{r}) = \frac{1}{\mu} \int_{S'} \tau_s(\mathbf{r}') g(\mathbf{r}, \mathbf{r}') dS', \quad (67)$$

where  $\tau_s$  are fictitious surface magnetic charges (dual to the electric charges). Equations (67) are dual to (24), and the surface magnetic currents are related to the magnetic charges by the continuity equation dual to equation (26),

$$\text{div}_s \mathbf{M}_s = -j\omega\tau_s. \quad (68)$$

The electric and magnetic field, in a homogeneous medium whose parameters are  $\epsilon$  and  $\mu$ , are expressed in terms of the four potentials as

$$\mathbf{E} = -j\omega\mathbf{A} - \text{grad } V - \frac{1}{\epsilon} \text{curl } \mathbf{F}, \quad \mathbf{H} = -j\omega\mathbf{F} - \text{grad } V_m + \frac{1}{\mu} \text{curl } \mathbf{A}. \quad (69)$$

Of course, for a vacuum, we have to use  $\epsilon_0$  and  $\mu_0$  instead of  $\epsilon$  and  $\mu$ , respectively. In contrast to equation (18), we deal here with the vector  $\mathbf{H}$  instead of  $\mathbf{B}$ , to stress the symmetry (duality) in relations for the vectors  $\mathbf{E}$  and  $\mathbf{H}$ . From the above equations, we can express the vectors  $\mathbf{E}$  and  $\mathbf{H}$  in terms of  $\mathbf{J}_s$  and  $\mathbf{M}_s$ .

The fields within  $S$  in Figure 16b are zero because the equivalent sources,  $\mathbf{J}_s$  and  $\mathbf{M}_s$ , along with the associated charges, annihilate the actual fields within  $S$ . Consequently, the fields produced by  $\mathbf{J}_s$  and  $\mathbf{M}_s$  within  $S$  are the negatives of the actual fields. If we consider the system of Figure 16c, where we have the negatives of  $\mathbf{J}_s$  and  $\mathbf{M}_s$  distributed over  $S$ , with all other field sources outside  $S$  removed, the resulting fields within  $S$  are the same as the original fields in Figure 16a. It can be proven that in Figure 16c the fields outside  $S$  are zero. Hence, the outside region can be assumed filled with the same medium as is inside  $S$ , and expressions for potentials (24) and (67) used again with the actual parameters of the dielectric body under consideration,  $\epsilon$  and  $\mu$ .

Following the above example, we shall outline the procedure for solving the scattering problem of the dielectric body shown in Figure 16a. We assume to know the impressed (illuminating) electric field ( $\mathbf{E}_i$ ). However, we do not know the actual induced polarization currents and charges, nor we know the equivalent surface electric and magnetic currents. The objective is to find the equivalent surface sources, as then we can evaluate the fields

produced (scattered) by the dielectric body. We simultaneously consider the systems of Figures 16b and 16c. In the system of Figure 16b the fields on the inner face of  $S$  are zero, as the fields at any point of the region encapsulated by  $S$  are zero. Hence, we can impose the condition that the tangential component of the electric field be zero on the inner face of  $S$ . This field is the sum of the illuminating field and the field produced by  $\mathbf{J}_s$  and  $\mathbf{M}_s$ . Using (69), the expressions for the potentials, and this boundary condition, we obtain one integral equation for  $\mathbf{J}_s$  and  $\mathbf{M}_s$ . Similarly, in the system of Figure 16c the tangential component of the electric field on the outer face of  $S$  can be imposed to be zero. This field is produced by the negatives of  $\mathbf{J}_s$  and  $\mathbf{M}_s$ , and this boundary condition yields another integral equation for  $\mathbf{J}_s$  and  $\mathbf{M}_s$ . Note that, compared with the case of a PEC body, we now have doubled the unknowns, i.e., we have two surface currents instead of one, but we have also doubled the number of boundary conditions. The resulting equations are EFIEs. In an analogous way, MFIEs can be derived. However, another approach, referred to as the PMCHW formulation [51], has been found to have certain advantages and it has been used more frequently than the EFIE and MFIE.

The resulting system of simultaneous integral equations can be solved using the MoM, following a similar procedure as for PEC bodies. Now we have to approximate both  $\mathbf{J}_s$  and  $\mathbf{M}_s$ . We can use similar basis functions for both currents and similar testing procedures for both integral equations.

This approach can be generalized to the case of an arbitrary number of homogeneous media. For an antenna problem, we need to include some metallic parts into the structure, like wires and plates. This can be done in a straightforward manner, but further details will be omitted here.

Based on the above outline, several techniques have been developed for solving antennas and scatterers with piecewise-homogeneous media. Two prominent techniques exist that are extensions of the PEC-body solutions. They are based on the triangular patches [52] and the bilinear surfaces with polynomial basis functions [53,32], respectively. The techniques based on the surface integral equations are considered to be the most efficient methods for the analysis of practical systems that consist of metallic and dielectric bodies. Generally, these methods are applicable not only to radiating structures, but also to virtually any electromagnetic field problem, including, for example, microwave components and circuits. However, they cannot treat problems that involve highly inhomogeneous and anisotropic materials.

#### 4.4.4. Finite-element method

The finite-element method is a technique that can be used to efficiently analyze electromagnetic structures that include inhomogeneous and anisotropic materials. We shall only outline this technique here. An extensive survey of the FEM can be found, for example, in reference [54].

As stated in Section 1, the FEM is based on solving for the field distribution, or, equivalently, solving for the potentials. The equation that is to be solved numerically is usually derived from differential form of Maxwell's equations following the so-called variational approach, which is equivalent to applying the Galerkin method. The region where the fields exist is divided into a large number of subdomains, which are of a finite size. Within each subdomain, the field or potential distribution is approximated by a basis function, which is, most often, a linear or a quadratic function. For 3D electromagnetic problems, the basis functions depend on three spatial coordinates.

Due to the finite size of the subdomains, the basic FEM is most suitable for the analysis of fields within an electromagnetically shielded region, like a microwave cavity or a shielded microwave circuit. In antenna problems, however, the space occupied by the fields is infinite. Hence, to analyze antennas, it is necessary to bypass the limitation of the finite-size subdomains. This can be done following two distinct approaches.

The first approach is to construct special basis functions on subdomains that extend to infinity. This technique has not been found suitable enough for antenna applications.

The second approach is to assume the region where the finite elements are distributed to be bounded by a finite closed surface,  $S$ . This surface encompasses all material inhomogeneities, to make an efficient use of the FEM. In radiation (antenna) problems, this surface must also simulate an infinite open space into which the antenna radiates. This simulation is performed in two ways.

The first way is to impose a local boundary condition on  $S$ . The simplest approach is to assume  $S$  to be a sphere located in the far-field region (referred to as the radiation sphere). In this case, the electric and magnetic field vectors are practically tangential to the sphere, they are mutually orthogonal, and they are related by the so-called radiation boundary condition, i.e., equation (56). In this case, the unit vector  $\mathbf{u}_r$  is the unit outward normal on  $S$ . The basic problem is to have  $S$  really far away, in the far-field zone, to be sure (56) is valid with a sufficient accuracy. This request may overly extend the size of  $S$ . Modifications of the radiation boundary condition have been constructed, collectively referred to as the absorbing boundary conditions, which yield good results for smaller-sized  $S$ , which also may have an arbitrary shape. Nevertheless, even for these modified conditions, there is a limitation of the size of  $S$ , and this surface may still need to be impractically large.

The second way is to use the so-called non-local boundary conditions. This is hybridization between the FEM and the surface integral equation approach described in Section 4.4.3. Thereby,  $S$  can have an arbitrary shape

and it can be shrunk to minimal dimensions sufficient to encompass all media inhomogeneities. We separately consider two problems, one for the region exterior to the surface  $S$ , and another for the region encapsulated by  $S$ . On the surface  $S$  fictitious electric and magnetic currents are placed following the same equivalence principles described in connection with equation (66) and shown in Figure 16b. For the exterior region these currents replace all field sources within  $S$ . An identical set of integral equations is formulated based on the boundary conditions as described in Section 4.4.3. For the interior region the classical FEM is applied, with finite-size elements. However, on  $S$  the negatives of the equivalent currents are placed, similarly as shown in Figure 16c, which replace the influence of the exterior region. The approximation for the equivalent surface currents is deduced from the finite elements. Appropriate boundary conditions are imposed on  $S$  requiring the field outside  $S$  be zero. The whole procedure results in a system of simultaneous equations, which ultimately yields the distribution of equivalent surface currents and the field distribution within  $S$ .

The FEM hybridized with the surface integral equations can handle antenna and scatterer problems that involve highly inhomogeneous and anisotropic media more efficiently than the volume integral equation approach described in Section 4.4.2. However, such systems are very rare in practical antenna designs. For piecewise-homogeneous and isotropic media the surface integral equation approach described in Section 4.4.3 is more efficient than the FEM because it involves a significantly smaller number of unknowns. Finally, the finite elements can not easily be accommodated to thin wires and plates. As the result, the FEM has not found a wider practical use for antenna applications.

#### 4.4.5. Example

As an example of the analysis of composite metallic and dielectric structures we consider the microstrip patch antenna shown in Figure 17a. The patch is almost a square: its dimensions are 57.6 mm by 58.8 mm, and it is designed for the GPS L1 band applications. It is printed on an FR-4 substrate, 1.59 mm thick. Measurements of the parameters of FR-4 in a wide frequency range have shown that its relative permittivity steadily decreases with frequency, whereas the loss tangent is fairly constant (about 0.02). At the GPS band the relative permittivity of the substrate is  $\epsilon_r = 4.3$ . The antenna is fed by a coaxial line, connected near one diagonal. Figure 17b shows measured results for the antenna reflection coefficient as a function of frequency along with results computed using the program of reference [32]. The agreement is excellent, bearing in mind the very narrow frequency band. Figure 17c shows the computed radiation pattern in a vertical plane. The numerical model takes into account the finite size of the ground plane, and it also includes effects of the surface waves in the dielectric, unlike many simplified techniques for the analysis of patch antennas.

## 5. Conclusion

This chapter presents the basic principles of the method of moments (MoM), emphasizing its applications to the analysis of antennas. This technique enables a computer simulation of practically arbitrary antennas whose dimensions range from a small fraction of the wavelength up to several tens or even hundreds of wavelengths. Details of the MoM can be found summarized in several excellent monographs, including [2,5-15]. Examples are given of various antennas illustrating the power of this technique and showing the degree of agreement between the theory and experiment that can usually be expected in practice.

The analysis presented in this chapter is for the steady-state sinusoidal regime. To complete the overview of numerical techniques, the reader should refer to the chapter devoted to finite-difference methods, which deals with the time-domain analysis, and to the chapter devoted to high-frequency techniques, which deals with techniques that are more efficient than MoM for electrically large structures. Finally, to gain more information about available software for the antenna analysis, including programs based on the MoM, the reader should refer to the corresponding chapter devoted to practical antenna design methods.

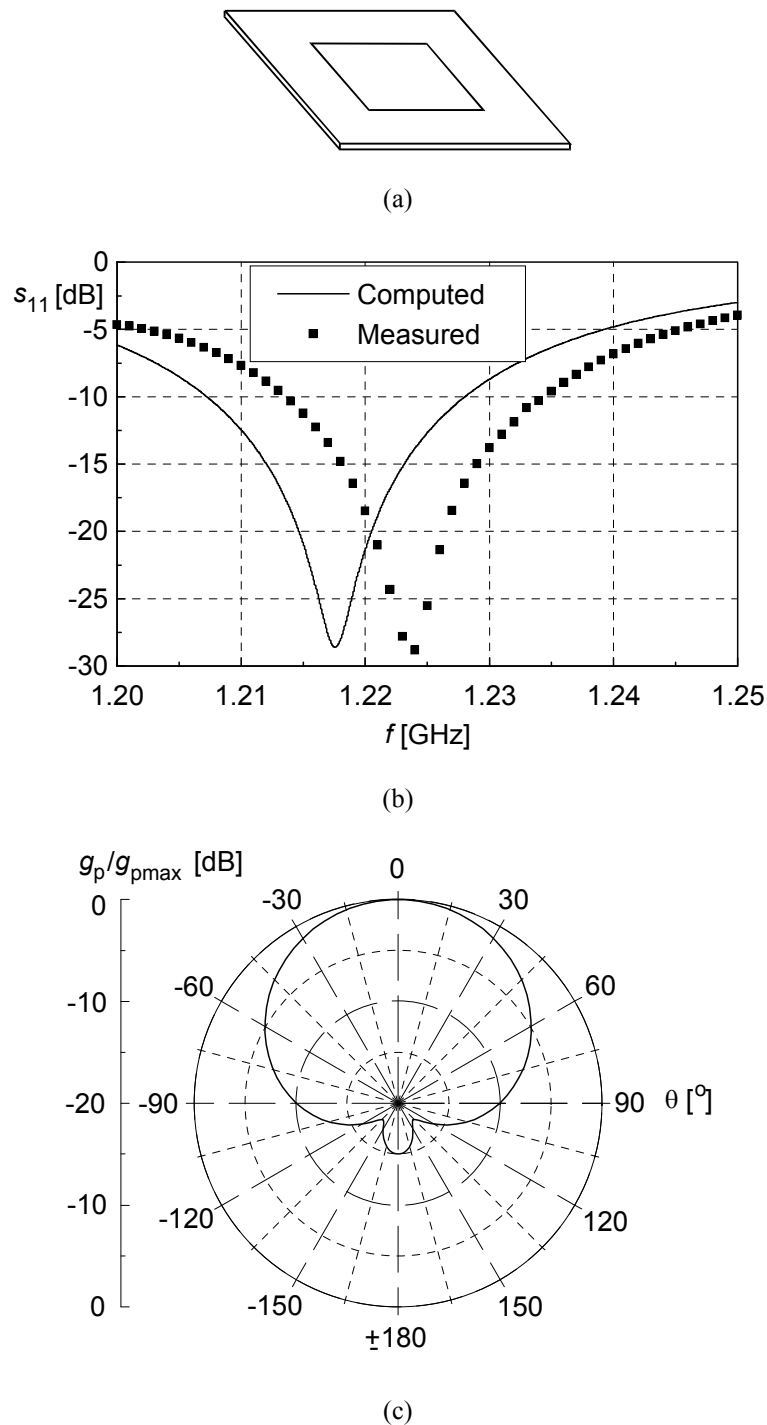


Figure 17. A microstrip patch antenna: (a) sketch, (b) input reflection coefficient with respect to  $50 \Omega$  ( $s_{11}$ ) as a function of frequency ( $f$ ), and (c) radiation pattern in a vertical plane at 1225 MHz: relative power gain ( $g_p / g_{pmax}$ ) as a function of zenith angle ( $\theta$ ).

## 6. Acknowledgment

Authors wish to thank the following staff and students of the Electromagnetic Group of the Faculty of Electrical Engineering, University of Belgrade, and staff of Intel Microwaves, Belgrade, for their help in preparing and performing experiments presented in this chapter (in alphabetical order): Dr. Radivoje Biljic, Professor Emeritus Dr. Momcilo Dragovic, Ms. Andjelija Ilic, B.Sc., Dr. Vladana Likar-Smiljanic, Mr. Miodrag Mikavica, M.Sc., Ms. Aleksandra Stekovic, B.Sc., Mr. Ivica Stevanovic, Professor Emeritus Dr. Jovan Surutka, Mr. Miodrag

Tasic, B.Sc., and Ms. Alenka Zajic. Authors also wish to thank Dr. Luca Niccolai, Managing Director of Dynaflex, S.R.L., Osimo, Italy, for courtesy to publish Figure 10.

## 7. References

- [1] R. Plonsey, R.E. Collin, *Principles and Applications of Electromagnetic Fields*, New York: McGraw-Hill, 1961.
- [2] R.F. Harrington, *Field Computation by Moment Methods*, Piscataway (NJ): IEEE Press, 1993.
- [3] R.F. Harrington, *Time-Harmonic Electromagnetic Fields*, New York: McGraw-Hill, 1961.
- [4] B.D. Popovic, "Electromagnetic field theorems (a review)," *Proc. IEE*, Pt. A, pp. 47-63, 1981.
- [5] R. Mittra (Ed.), *Computer Techniques for Electromagnetics*, Elmsford, NY: Pergamon Press, 1973.
- [6] R. Mittra (Ed.), *Numerical and Asymptotic Techniques in Electromagnetics*, New York: Springer Verlag, 1975.
- [7] B.J. Strait (Ed.), *Application of the Method of Moments to Electromagnetic Fields*, St. Cloud, FL: The SCEEE Press, 1980.
- [8] J. Moore and R. Pizer, *Moment Methods in Electromagnetics: Techniques and Applications*, New York: John Wiley and Sons, 1984.
- [9] T. Itoh (Ed.), *Numerical Techniques for Microwave and Millimeter-Wave Passive Structures*, New York: John Wiley and Sons, 1990.
- [10] R.C. Hansen (Ed.), *Moment Methods in Antennas and Scattering*, Boston: Artech House, 1990.
- [11] J.H.H. Wang, *Generalized Moment Methods in Electromagnetics*, New York: John Wiley and Sons, 1991.
- [12] E.K. Miller, L. Medgyesi-Mitschang, and E.H. Newman (Eds.), *Computational Electromagnetics: Frequency-Domain Method of Moments*, Piscataway, NJ: IEEE Press, 1992.
- [13] N. Morita, N. Kumagai, and J. Mautz, *Integral Equation Methods for Electromagnetics*, Boston: Artech House, 1992.
- [14] K. Umashankar, *Computational Electromagnetics*, Boston: Artech House, 1993.
- [15] A. Peterson, S.C. Ray, and R. Mittra, *Computational Methods for Electromagnetics*, New York: IEEE Press and Oxford: Oxford University Press, 1998.
- [16] W. R. Smythe, *Static and Dynamic Electricity*, New York: McGraw-Hill, 1968.
- [17] T.K. Sarkar, K.R. Siarkiewicz, and R.F. Stratton, "Survey of numerical methods for solution of large systems of linear equations for electromagnetic field problems", *IEEE Trans. Antennas Propagat.*, vol. AP-29, pp. 847-856, Nov. 1981.
- [18] T.K. Sarkar, *Application of the Conjugate Gradient Method in Electromagnetics and Signal Processing*, New York: Elsevier Science Publications, 1991.
- [19] T.K. Sarkar, E. Arvas, "Application of FFT and the conjugate gradient method for the solution of electromagnetic radiation from electrically large and small conducting bodies", *IEEE Trans. Antennas Propagat.*, vol. 34, pp. 635-640, May 1986.
- [20] T.K. Sarkar, A.R. Djordjevic, and E. Arvas, "On the choice of expansion and weighting functions in the numerical solution of operator equations", *IEEE Trans. Antennas Propagat.*, vol. AP-33, pp. 988-996, Sept. 1985.
- [21] B.D. Popovic, M.B. Dragovic, and A.R. Djordjevic, *Analysis and Synthesis of Wire Antennas*, Chichester, England: Research Studies Press (a division of John Wiley and Sons), 1982.
- [22] B.M. Kolundzija, "Comparison of a class of sub-domain and entire-domain basis functions automatically satisfying KCL", *IEEE Trans. Antennas Propagat.*, vol. AP-44, pp. 1362-1366, Oct. 1996.
- [23] P.C. Waterman, "Matrix formulation of electromagnetic scattering", *Proc. IEEE*, vol. 53, pp. 805-812, 1965.
- [24] Y. Leviatan, A. Boag, and A. Boag, "Generalized formulations for electromagnetic scattering from perfectly conducting and homogeneous material bodies-theory and numerical solution", *IEEE Trans. Antennas Propagation*, vol. AP-36, pp. 1722-1734, Dec. 1988.
- [25] E.K. Miller and F.J. Deadrick, "Some computational aspects of thin-wire modeling", in R. Mittra (Ed.): *Numerical and Asymptotic Techniques in Electromagnetics*, Berlin: Springer-Verlag, 1975.
- [26] B.D. Popovic and A. Nesic, "Generalization of the concept of equivalent radius of thin cylindrical antennas", *Proc. IEE*, Pt. H, pp. 153-159, 1984.
- [27] A. Baños, *Dipole Radiation in the Presence of a Conducting Half-Space*, New York: Pergamon Press, 1966.
- [28] W.A. Imbraile, "Applications of the method of moments to thin-wire elements and arrays", in R. Mittra (Ed.), *Numerical and Asymptotic Techniques in Electromagnetics*, Berlin: Springer Verlag, 1975.
- [29] J. Rockway, J. Logan, D. Tam, and S. Li, *The MININEC SYSTEM: Microcomputer Analysis of Wire Antennas*, Boston: Artech House, 1988.

- [30] J.H. Richmond, *Radiation and Scattering by Thin-Wire Structures in the Complex Frequency Domain*, OSU Research Foundation Report RF 2902-10, 1973.
- [31] A.R. Djordjevic, M.B. Bazdar, T.K. Sarkar, and R.F. Harrington, *AWAS for Windows: Analysis of Wire Antennas and Scatterers, Software and User's Manual*, Boston: Artech House, 1995.
- [32] B.M. Kolundzija, J.S. Ognjanovic, and T.K. Sarkar, *WIPL-D: Electromagnetic Modeling of Composite Metallic and Dielectric Structures, Software and User's Manual*, Boston: Artech House, 2000.
- [33] A.R. Djordjevic, B.D. Popovic, and M.B. Dragovic, "A method for rapid analysis of wire-antenna structures", *Archiv für Elektrotechnik*, vol. 61, pp. 17-23, Jan. 1979.
- [34] B. M. Kolundzija and B. D. Popovic, "Entire-domain Galerkin method for analysis of generalized wire antennas and scatterers", *Proc. IEE*, Pt. H, vol. 139, pp. 17-24, Feb. 1992.
- [35] A.R. Djordjevic, L.N. Niccolai, and T.K. Sarkar, "Vehicular antenna for AM/FM radio, mobile phone, and GPS", *Proc. of Millennium Conf. on Antennas Propagat. (AP2000)*, Davos, April 2000.
- [36] C.D. Taylor and D.R. Wilton, "The extended boundary condition solution of the dipole antenna of revolution", *IEEE Trans. Antennas Propagat.*, vol. AP-22, pp. 407-413, May 1974.
- [37] S.M. Rao, D.R. Wilton, and A.W. Glisson, "Electromagnetic scattering by surfaces of arbitrary shape", *IEEE Trans. Antennas Propagat.*, vol. AP-30, pp. 409-418, May 1982.
- [38] B.M. Kolundzija and B. D. Popovic, "Entire-domain Galerkin method for analysis of metallic antennas and scatterers", *Proc. IEE*, Pt. H, vol. 140, pp. 1-10, Feb. 1993.
- [39] J.C. Monson and N.J. Damaskos, "A scheme for eliminating internal resonances: the parasitic body technique," *IEEE Trans. Antennas Propagation*, vol. AP-42, pp. 1089-1096, Nov. 1982.
- [40] A.J. Poggio and E.K. Miller, "Integral equation solutions of three-dimensional scattering problems", in R. Mittra (Ed.): *Computer Techniques for Electromagnetics*, Oxford: Pergamon Press, 1973.
- [41] J.R. Mautz and R.F. Harrington, "H-field, E-field and combined-field solutions for conducting bodies of revolution", *A.E.Ü.*, vol. 32, pp. 157-164, 1978.
- [42] E. H. Newman and D. M. Pozar, "Electromagnetic modeling of composite wire and surface geometries", *IEEE Trans. Antennas Propagat.*, vol. AP-26, pp. 784-789, Nov. 1978.
- [43] B.M. Kolundzija and B.D. Popovic, "General localized junction model in the analysis of wire-to-plate junctions," *Proc. IEE*, Pt. H, vol. 141, pp. 1-7, Feb. 1994.
- [44] B. Kolundzija, J. Surutka, and B. Miletic, "New approach to the design of TV panel antenna for UHF frequency range", *Proc. of XLIII Yugoslav ETRAN Conf.*, Zlatibor, pp. 25-32, Sept. 1999.
- [45] K. Liu, C. A. Balanis, C. R. Birtcher, and G. C. Barber, "Analysis of pyramidal horn antennas using moment methods", *IEEE Trans. Antennas Propagat.*, vol. 41, pp. 1379-1388, Oct. 1993.
- [46] J.H. Richmond, "Scattering by a dielectric cylinder of arbitrary cross section shape", *IEEE Trans. Antennas Propagat.*, vol. AP-13, pp. 334-341, Mar. 1965.
- [47] D. E. Livesay and K. M. Chen, "Electromagnetic fields induced inside arbitrarily shaped biological bodies," *IEEE Trans. Microwave Theory Tech.*, vol. MTT-22, pp. 1273-1280, Dec. 1974.
- [48] H. Schaubert, D.R. Wilton, and A.W. Glisson, "A tetrahedral modeling method for electromagnetic scattering by arbitrarily shaped inhomogeneous dielectric bodies", *IEEE Trans. Antennas Propagat.*, vol. AP-32, pp. 77-85, Jan. 1984.
- [49] T.K. Sarkar, E. Arvas, and S. Ponnappalli, "Electromagnetic Scattering from Dielectric Bodies", *IEEE Trans. Antennas Propagat.*, vol. AP-37, pp. 673-676, May 1989.
- [50] B.M. Notaros and B.D. Popovic, "Large-domain integral-equation method for analysis of general 3-D electromagnetic structures", *IEE Proc. Microw. Antennas Propag.*, vol. 145, pp. 491-495, Dec. 1998.
- [51] J.R. Mautz and R.F. Harrington, "Electromagnetic scattering from a homogeneous material body of revolution", *A.E.Ü.*, vol. 33, pp. 71-80, 1979.
- [52] S.M. Rao, T.K. Sarkar, P. Midya, and A.R. Djordjevic, "Electromagnetic radiation and scattering from finite conducting and dielectric structures: surface/surface formulation", *IEEE Trans. Antennas Propagat.*, vol. AP-39, pp. 1034-1037, July 1991.
- [53] B.M. Kolundzija, "Electromagnetic modeling of composite metallic and dielectric structures", *IEEE Trans. Microwave Theory Tech.*, vol. MTT-47, pp. 1021-1032, July 1999.
- [54] M. Salazar-Palma, T.K. Sarkar, L.E. Garcia-Castillo, T. Roy, and A.R. Djordjevic, *Iterative and Self-Adaptive Finite-Elements in Electromagnetic Modeling*, Boston: Artech House, 1998.